/
Article / Book Information

( )	
Title(English)	Study on Surface-controlled Functional Oxides with Encapsulated Spherical Shell Structures
( )	
Author(English)	Ryuma Malik Matsuda
( )	: , : , : 10184 , :2016 3 26 , : , : , , , ,
Citation(English)	Degree:, Conferring organization: Tokyo Institute of Technology, Report number: 10184 , Conferred date:2016/3/26, Degree Type:Course doctor, Examiner:,,,,
( )	
Type(English)	Doctoral Thesis

A doctoral dissertation

Study on Surface-controlled Functional Oxides with Encapsulated Spherical Shell Structures

Ryuma Malik Matsuda

Supervised by

Professor Osamu Odawara

Associate Professor Hiroyuki Wada

Department of Innovative and Engineered Materials

Interdisciplinary Graduate School of Science and Engineering

Tokyo Institute of Technology

March 2016

Contents

Chapter 1 General introduction

1.1 Modern applications of capsule

Capsule is generally defined as a shape-formed product where various phase core materials covered by a solid shell in the broad sense of the word. Figure 1.1 shows examples for the capsule form with each core phase. Each capsule having different core phases (solid, liquid, gas or hollow core) represents well-known products in daily. The capsule covered by a soft shell must need the core to form the capsule, while it is possible to retain the capsule formation with a hard shell.

	Core			
	Solid	Liquid	Gas	Hollow core
Soft shell	Sugar coated confectionary	Artificial salmon roe	Balloon	—
Hard shell	Golf ball	Two-piece drug	Tennis ball	Ping-pong ball

Figure 1.1 The various core phases capsule covered by soft shell or hard shell

The formation of capsule is mainly indicated as a spherical form with diverse size, thickness and porosity. Each specific structure will be decided by a purpose in which the capsule will be utilized. According to fields which has been studied and developed, several names are given, for instance, a core-shell [1], coated particle [2], micro [3] or nano capsule [4] and hollow sphere [5]. The capsule had been appeared in ancient time as an ingestion product covering by a gelatin at the head of a capsule history [6]. From around 18th century, a coated drug was appeared in order to avoid unpleasant taste of drug. As for further practical use, the micro capsule is well-known as that a first development applied for a carbonless copy paper with oil containing capsules was reported by B.K. Green and L. Schleicher [7]. Thank of tremendous contributions to the present, wide variety of works and applications with capsule have been explored. Figure

1.2 simply shows the time flow of the capsule development. In present day, there exist multiple applications as described below.
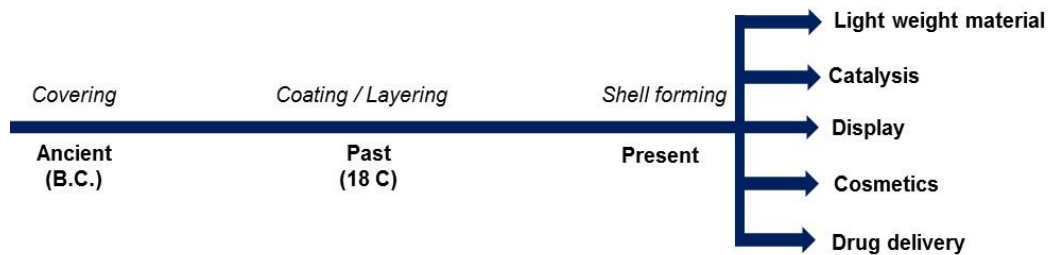
Figure 1.2 History of capsule development

One of applications is a protection media where core materials are protected by a durable shell or controlled to disperse at specific timing. This functionality has been developed in the basis of first concept of capsule utilization and often designed by organic shell. Other aspect of applications is an interactive media where the solid shell of capsule affects an ambient environment and more realized with a metal or ceramic shell. This functionality also can be categorized in the field of porous materials. Most of this functionality is competed with a foamed body which is also regarded as one of porous materials. The foamed body is generally produced by the integral molding, however, the variation of porous state due to nonhomogeneous void place and size in the body tends to occur which leads to the nonhomogeneous quality of characteristics (Figure 1.3). On the other hand, the porous state of capsule can be more precisely designed by controlling the inner core space and porosity in the shell with tunable filling property and shape of composite consisting of capsules. As for the disadvantages, a nonhomogeneous capsule shape or size might happen in dependent on the fabrication methods. However, owing to attractive advantages, the functionality for the interactive media has been enthusiastically studied as a new concept of capsule utilization.

	Advantage		**Disadvantage**	
Foamed body	Integral molding		Nonhomogeneous void place and size	
Capsule	· Detailed porous design · High shape selectivity · High filling property		Nonhomogeneous capsule size and shape	
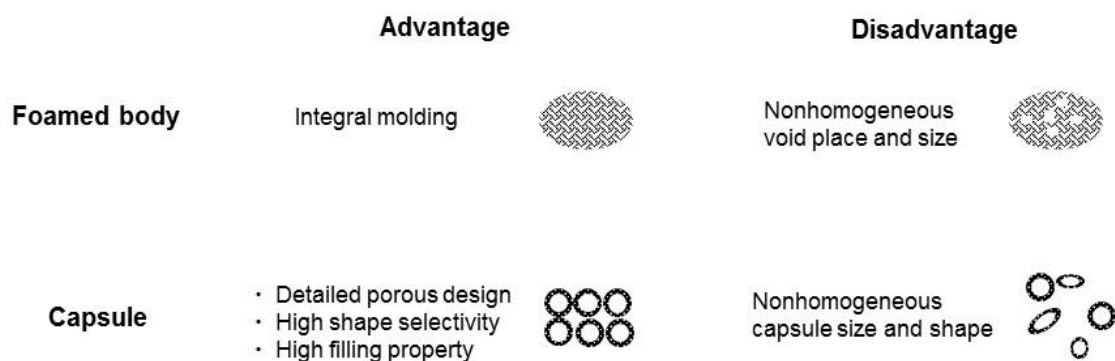
**Figure 1.3** Advantage and disadvantage for the foamed body and capsule

1.1.1 Protection media

Biological application

   In capsule study, it is not an exaggeration to say that a medical application laid the foundation for the capsule history. A coated or sealed medicine has become a common sense in a pharmaceutical field. By adding some flavors in the shell material, it will be easy for people taking the medicine as well as the protection behavior. Other purpose of the coating is that a sustained release of core medicine. The shell materials are possible to dissolve gradually in a digestive system, the core medicine will be dissolved at specific area and time to promote its efficacy. There are 2 basic types of pharmaceutical capsules: Two-piece capsule (hard capsule) and single-piece capsule (soft capsule) [8]. The two-piece capsule consists of a body and cap which have one-side-closed cylindrical shape. The cap has larger diameter than that of body and fits the body to seal an ingredient. On the other hand, the single-piece capsule sometimes can have a seamless shape owing to the production method. Both of pharmaceutical capsule generally are made of gelatin. If the gelatin contains a plasticizer such as glycerol or sorbitol, the elasticity of gelatin will increase [9]. This is the basic concept to make a soft shell for the single-piece capsule. They are used properly depending on the type of ingredient to be sealed or when it releases the ingredient. For example, the hard capsule is suit to contain the solid and liquid ingredients, while the soft capsule is suit to

contain the liquid ingredient with flexible shape selectivity. The concept of the sustained release leads to design a drug delivery system with a lot of attentions in recent study (Figure 1.4). Especially it is regarded as a new attractive treatment for the cancer owing to possible local treatment without damaging other normal cell. There are some transfer types to realize this concept. Firstly, a natural transfer type by utilizing the immune system in the body [10], because the cancer cell intensively absorb the particles flowing in the blood vessel which is called enhanced permeability and retention effect [11]. Therefore, the drug capsule can be injected to the blood vessel and just relied on the blood flow. Since the capsule is flowed in the blood vessel and accumulated in the cancer cell, it should be designed in a submicron scale. Secondly, a transfer by external force such as magnetic force is used to induce the way to the destination [12]. This type of capsule includes or consisted of the magnetic materials. Thirdly, the capsule having a motive power can move by itself [13]. This type is based on the electric power and capsule directly aims to the destination. It seems like a considerable small submarine. As for the treatment, the dispersed drug from the capsule works [10] or capsule heat and thermally damages the cancer, so called hyperthermia effect [14].
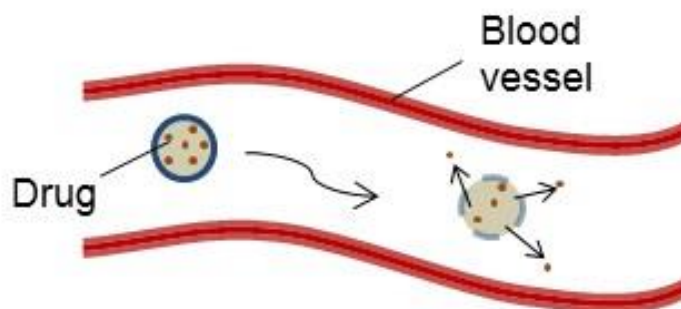
**Figure 1.4** The image for drug delivery system by using drug containing capsule

Display

The concept of the carbonless copy paper has been inherited as a functional display device using microcapsule has been appeared [15]. The device is usually paper form where the capsules containing chargeable particle with dye disperse. When an

electric power or electric field are applied to the paper, its surface will change the color since the particles go along the direction involving an electric force (Figure 1.5). Therefore, such paper-like device is sometimes called "electric paper (e-paper)". The e-paper is rewritable and erasable, therefore it can compete with an ordinary paper in terms of saving resources.
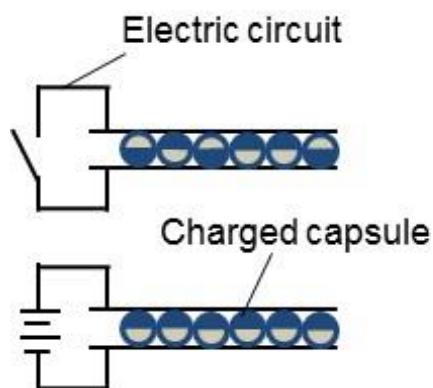
Figure 1.5 The image of electric paper by using chargeable particle containing capsule

1.1.2 Interaction media

High catalytic activity

Since the capsule has inner core with fine size in comparison with solid particle, surface activity involving the adsorption is facilitated due to high specific surface area [16]. It will result the promotion of a conversion activity for catalysis (Figure 1.6). Because the capsule shell is made of solid, a heterogeneous catalysis has been applied. It is possible to use as catalyst support where the fine catalyst materials with size of dozens of nanometers is located on the surface of capsule shell as well as being catalyst itself [17]. The surface covering by fine catalysts sometimes leads to decrease the specific surface area compared with that of as-prepared support material. However, by introducing a zeolite coating on the solid particle catalyst, high specific surface area up to hundreds of square meter per gram retains due to fine pores on the zeolite [18]. It leads to promote the diffusion of material or electron which is influence on the catalytic activity. Therefore, there are 2 types of catalyst capsule forms as

described above. The former case is based on hollow type capsule with considerable fine size, the latter case is based on solid core type capsule with considerable high specific surface area shell.
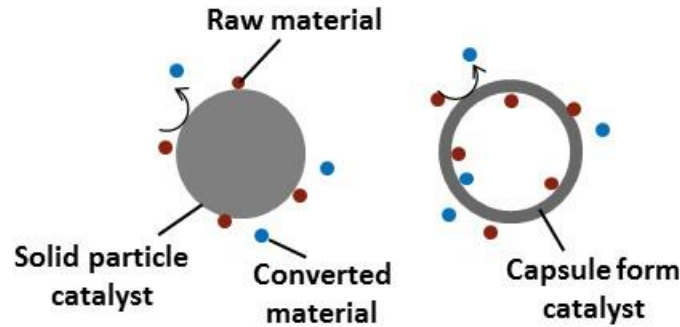
Figure 1.6 The image of catalytic activity promotion by using solid particle catalyst (left) and hollow capsule form catalyst (right)

Thermal insulation

The thermal insulation is a key technology to solve a problem relating to the temperature distribution. It is essential for our life to keep a warm environment or protect from severe temperature. Especially, the fine size hollow capsule is possible to apply for this technology. The existence of core inner space mostly relates to the decreasing of thermal conductivity over the capsule body. It means the temperature is not immediately varied. For instance, the hollow capsule with silica based shell and size of a few hundred nanometers exhibited very low thermal conductivity around 0.020 W/mK [19]. By collecting the capsules, the desired shape composite can be fabricated (Figure 1.7).
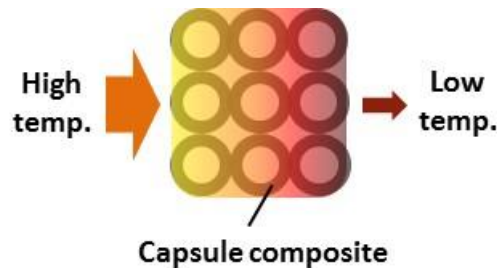
Figure 1.7 The thermal insulation composite consisting of hollow capsules

1.2 Encapsulation techniques

The applications introduced in the section of 1.1 could be possible with multiple elaborate encapsulation techniques. In this section, 4 categorized processes to produce the capsules are explained with 2 representative methods for each process and the general mechanisms. Firstly, a direct sealing process is that shell material directly covers the core material. Secondly an expansion process is suit to produce a gas core capsule with an expansion force caused by generated gas product during the process. Thirdly, a precipitation process is made through the precipitation of shell material at a boundary between raw materials in dependent on the variation of pH, temperature or concentration. Lastly, a powder coating process is that the shell materials coat on the core materials by a mixing of raw materials. This process is based on most simple procedure to produce the capsule containing the core material with various phases. In the dissertation, the encapsulation mechanism for the powder coating process is particularly explained in detail.

1.2.1 Direct sealing process

Extrusion method

This process is generally made possible with the combination of coaxial nozzle and shell solidification from liquid state as briefly shown in Figure 1.8. The solidification is generally relied on the drying of the gelatin [20] or a crosslinking of alginate [21]. It is excellent method for the continuous generation of capsules containing various liquid materials. The method mostly has applied to the drug encapsulation. The precise condition of capsule structure such as homogeneous coating shell and size is possible owing to the contribution related to an innovation of fabrication machine. Although the direct sealing process, the capsule diameter can be precisely controlled up to 10 micrometer [22].
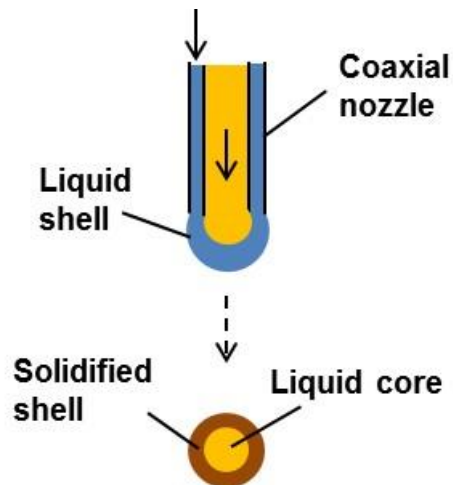
Figure 1.8 The liquid encapsulation by extrusion method

Filling method

The filling method has been adopted mainly in pharmaceutical industry to fabricate capsule containing drug ingredients. The capsule form consists of the body and cap as introduced in 1.1.1 and is mostly elliptical shape. Both of liquid and solid can be filled in the hard capsule. In the industry, tremendous number of capsules is fabricated through continuous process by using filling machine. It is said that 200,000 numbers of hard capsules every one hour can be produced [23]. The body created in advance is set the machine and core material is added in the body. Finally, the open edge is sealed with the cap as shown in Figure 1.9.
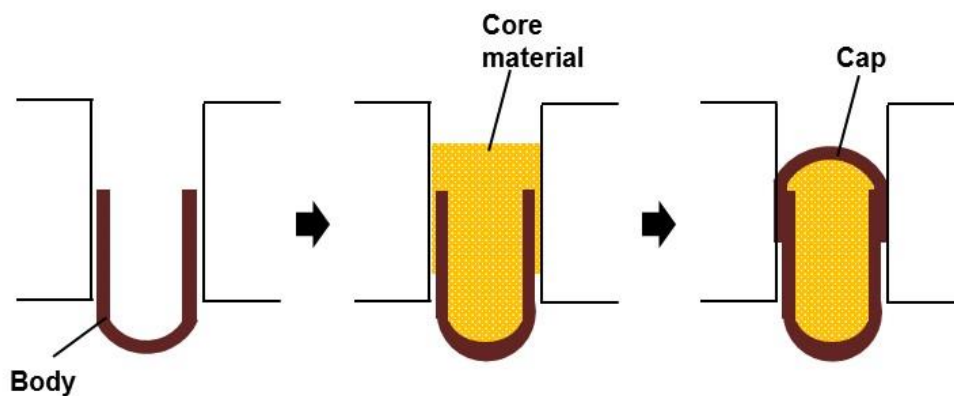
Figure 1.9 The encapsulation process of filling method

1.2.2 Expansion process

Spray dry method

The raw material solution is spayed along the flow of rapid stream gas from an atomizer (Figure 1.10). The atomized solution droplets are dispersed in a drying chamber which is generally heated at specific temperature. As a result, the surface of droplet is dried and solidified. This is the conventional way to obtain the dried product where the ingredients are homogeneously dispersed in the product particle. It is widely used in food industry and produces well-known product such as a skimmed milk powder [24]. In order to achieve the capsule form, the raw material solution should be the emulsion system containing a foaming agent prior to the spray drying [25]. It leads to expand the solution droplets during the spray dry. Therefore, the obtained product is possible to form the hollow type capsule.
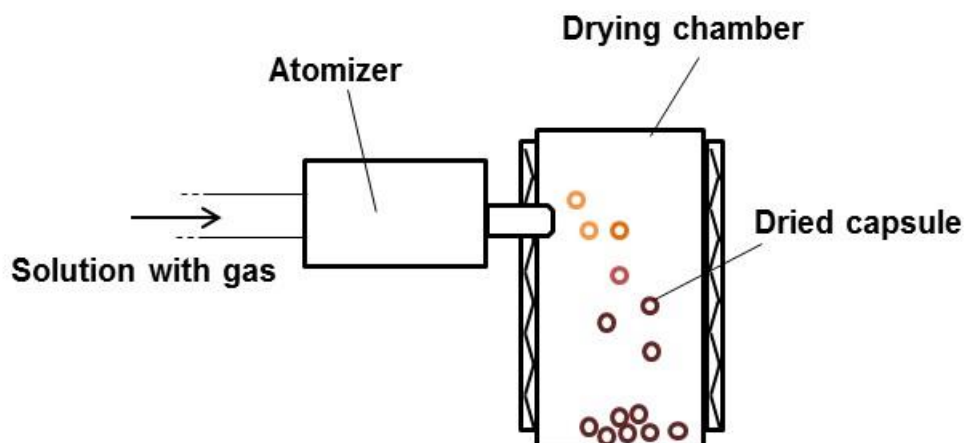
Figure 1.10 The outline installation of spray dry method

Ostwald ripening method

The hollow core or rattle type capsule where the solid core separately exists inside the capsule can be formed by Ostwald ripening method [26]. It is interesting encapsulation method by using chemical driving force. This phenomenon is driven by a difference of stability between 2 particles having different sizes in the nucleation or crystallization processes [27]. Since the smaller size particle is less energetically stable

compared to the larger size particle, it results in the promotion of particle size growth of larger particle by taking in the smaller size particle. The fine scale hollow capsule up to hundreds nanometers can be fabricated via the rattle type form from solid micro particle as shown in Figure 1.11 [26]. Similar concept for the preparation of hollow core capsule has been studied which is focused on Kirkendall effect where the difference of a diffusion rate of atom exiting in a material consisted of other atoms causes an unbalanced growth speed of synthesis [28]. As a result, the hollow core is formed inside either material particle which is occurred the slower product growth [29].

Figure 1.11 The hollow core capsule formation process by Ostwald ripening method

1.2.3 Precipitation process

Emulsion method

The emulsion method has been used to fabricate the liquid core capsule by precipitation or polymerization processes. These processes occur at the boundary between an oil phase and aqueous. As a result, solid shell is appeared at the boundary as shown in Figure 1.12. A driving force of the precipitation or polymerization is temperature or pH variation in the solution. Therefore, it is suit to be applied making the organic shell capsule. The capsule structure is influenced by the experimental condition such as type and concentration of raw material or pH [30]. It is also possible to make fine capsule up to hundreds of nanometers [30]. However, the shape selectivity is limited due to relying on self-growth formation which results in the spherical capsule because of the lowest surface energy. In the Figure 1.12, the liquid core capsule is formed from oil in water emulsion system [31]. On the other hand, it is also applied to

produce the rattle-type capsule from water in oil emulsion [32]. In addition, there exists a multiple phase system such as oil in water in oil [33] for making a hybrid capsule.
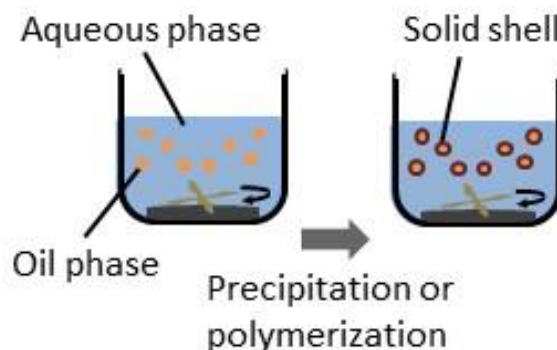
Figure 1.12 The liquid encapsulation by emulsion method

Bubble template method

　　　The bubble template method is quite new encapsulation method and based on epoch-making idea for making of hollow core capsule (Figure 1.13). It is said that this method is ecofriendly to fabricate the capsule due to unnecessity of core material which is needed to remove after the shell formation. The shell formation is occurred with the variation of pH leading to the precipitation [34] or contacting with the raw materials [35]. For instance, vaporized cyanoacrylate is added in the water, and then the solid shell is formed at the surface between bubble of cyanoacrylate monomer and solution. The shell formation is based on the polymerization of cyanoacrylate where the cyanoacrylate monomer rapidly reacts with water and the polymer is generated [35]. There is also a technical issue in terms of low material selectivity because the core material must be gas phase and reacts with the external environment to form the solid shell.
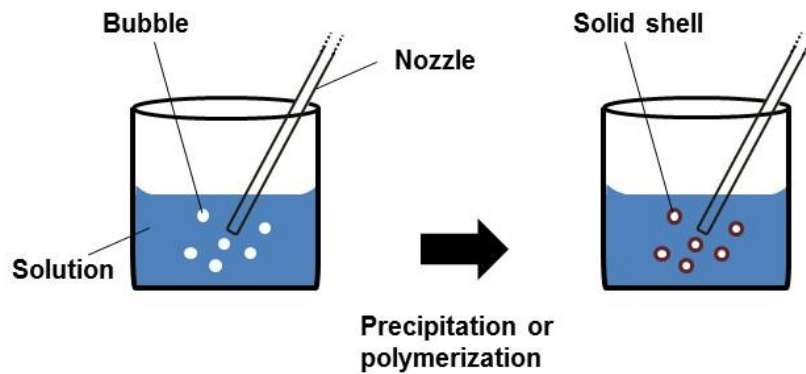
Figure 1.13 The hollow core capsule formation by bubble template method

1.2.4 Powder coating process

Dry water method

Dry water method is quite simple method to encapsulate the liquid where only the blending of hydrophobic powder and aqueous liquid is needed (Figure 1.14). Numerous encapsulated liquid droplets covered by the hydrophobic powder can be obtained. It is said that this powder-like liquid is possible to retain high amount of water up to 98 weight percent [36]. Each encapsulated liquid is made up of a capillary force between hydrophobic powder and liquid. Therefore, there is a limited diameter to retain the spherical shape. The capsule having large diameter forms the elliptical shape since the gravity force dominates and the power balance between it and the capillary force is collapsed [37].
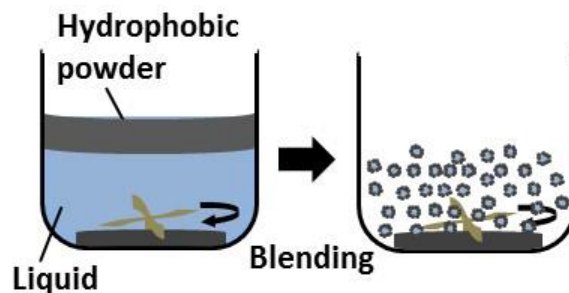
Figure 1.14 The liquid encapsulation by Dry water method

In order to achieve the encapsulation, a hydrophobicity of shell powder and blending condition are key factors [36] as indicated in Figure 1.15. If the powder is hydrophilic which means that a contact angle of water droplet on powder surface is less than 90 degree, the mixture state will form a suspension where the powder disperses in water. Although the powder is hydrophobic, the mixture is completely separated to each part (Di-phasic) when the blending energy is not enough to split the mixture well. The blending energy depends on multiple conditions such as a shearing speed or blade type [36]. If an enough blending energy is provided to the mixture, 2 types of results will be obtained. The capsule form is the one of them, however, a mousse form is also possible to get when the blending energy exceeds the immersion energy of the powder. The immersion energy means that a required energy for the powder to immerse into liquid from the air. Therefore, the encapsulation is attained under the optimum conditions.
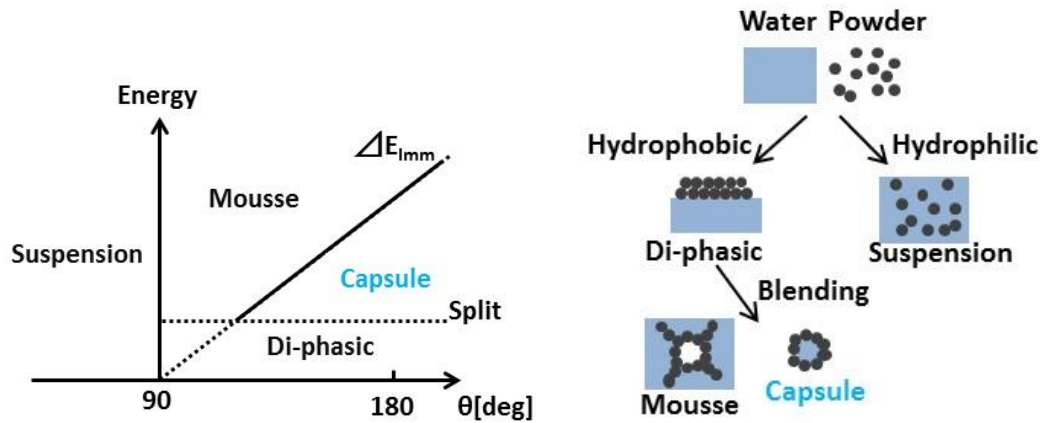
Figure 1.15 Mixture state of powder and water as a function of blending energy and contact angle of water droplet on powder surface (left), and the illustration for each mixture state (right) (ΔE_{imm} is immersion energy)

Sacrificial template method

The sacrificial template method is generally used to make hollow core capsule through a coating process and core removal process. This method includes 2 different starting systems: liquid based system and solid based system. The liquid based system is

suite to prepare fine size capsule. A spherical silica [38] or polystyrene [39] template are mostly used because they can be removed by pH or temperature variation. Here, detailed information about the solid based system is described below. The solid based system is usually indicated as the combination of powder coating process and heating process for the core removing. It is similar to a pan coating method for a layering of confectionery in terms of the coating process [40]. The coating state is considered to be formed with an ordered mixing phenomenon as shown in Figure 1.16 [41]. To achieve the ordered mixing, the difference between the diameter of small particles and large particles is needed to be large enough to increase the adhesion force of small particles against large particles. As for the template, expanded polystyrene spheres which are one of the foamed plastic are generally used because they are broadly and commercially produced. By covering the expanded polystyrene spheres with the powders which are mainly ceramics, the coating spheres are obtained. In this case, the expanded polystyrene sphere and powder should be much different in size to attain the homogeneous coating.
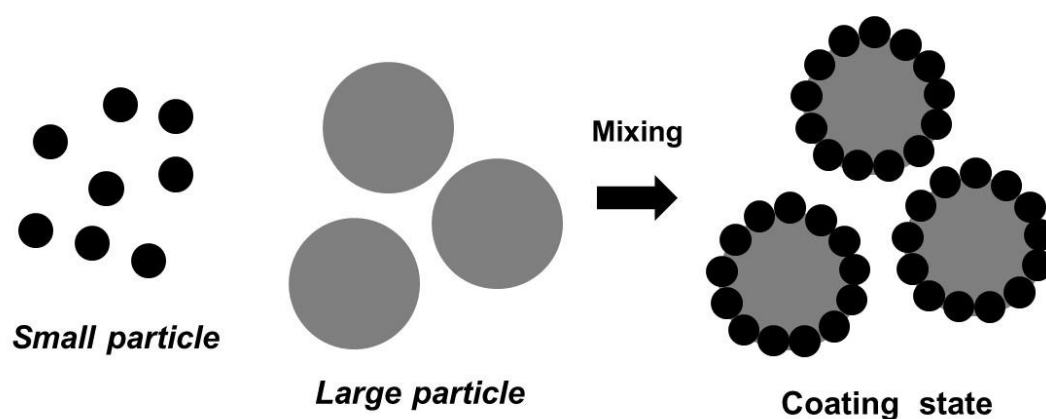
Figure 1.16 Coating of small particles on large particles by mixing

An organic binder which affects the retention of spherical form is also needed to mix during the coating process. By adding the optimum type and amount of the organic binder, the spherical form of capsule can be retained during the core removing. The core

can be removed by dissolution with some acids or heating in high temperature. Particularly, the heating process is not only to lead a pyrolysis of the template and organic binder, but the ceramic powder is sintered to promote a hardness of shell structure (Figure 1.17).
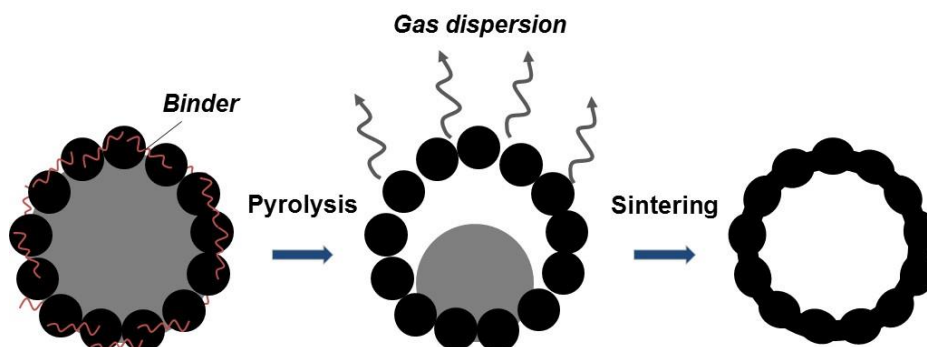
Figure 1.17 The schematic process to obtain hollow capsule under heating condition

1.3 Shell structure functionality and controllability

The functionality of capsule is highly dependent on the shell structure as well as the physicochemical property of shell material. Therefore, the shell structure is one of key factors for the application of capsule. The shell structure affects the capsule size, shell thickness and porosity. For instance, the shell size will be important when the capsule is applied to the biological field, the shell with large thickness and small porosity will express a large hardness to maintain the capsule structure and keep the core material protect. Besides, if the core material should be taken out, some methods such as crushing of shell or modification of shell geometry will be needed. This is particularly important for a liquid core capsule. The purpose of the liquid protection from external environment by the encapsulation is to prevent from a liquid dispersion and absorption of other factors into liquid. The prevention of liquid dispersion is effective for a good handling as solid-like form and suppression of decreasing the liquid amount due to the vaporization. The prevention of absorption of other factors involving materials, temperature or electromagnetic wave is also effective to keep the quality of

19

liquid core material. Especially, the prevention of liquid dispersion is deeply related to the capsule size. According to the thermodynamics, a flow in the liquid with small volume is hard to occur which leads to be utilized as the suppression of convection under heating condition. It simultaneously brings out a result of the liquid vaporization due to large surface area. However, by covering the liquid with shell, the vaporization also can be suppressed. In addition, the shell having numerous voids would control the dispersion ratio of the liquid and the difference of thermal conductivity between the liquid and shell material can promote the heat energy given to the liquid. It would lead to decrease the energy consumption. This concept will be utilized for heating of reactive material such as a liquid fuel. By encapsulating the reactive liquid droplets, long time heating to occur the reaction and high pressure to produce the fine fuel droplets [42] will be unnecessary (Figure 1.18). There is also similar concept in the field such using a micro reactor where the small volume of fluid is introduced in micro scale vessel in order to control and investigate the reaction in detail [43]. Particularly, in similar application of liquid capsules under heating condition, capsules containing phase change materials have been studied to realize the thermal storage resource [44]. The capsule shell is used as the vessel to protect inner liquid and thermally insulated. Thus, it is also meaningful to focus on the liquid capsule to be used for and open the thermal application.
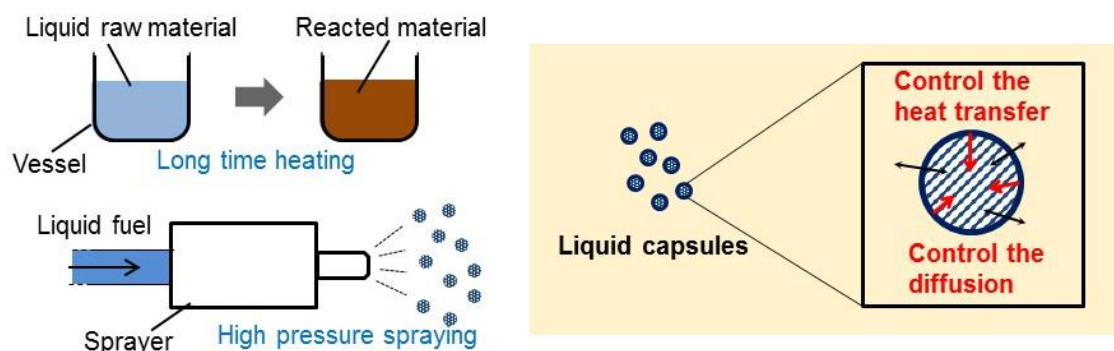
Figure 1.18 Advantage of liquid encapsulation in heating applications

Next, the shell structure controllability is explained as follows. The shell structure is key characteristic of capsule since it highly affects the capsule functionality. The formation of shell structure depends on the encapsulation methods and their conditions. In Figure 1.19, two fundamental methods to control the shell structure in terms of the variation of porous state are focused on. An etching method varies the shell structure by contacting to acidic or alkaline environments [45]. If the intensive etching is conducted, it significantly causes the porosification of shell structure [45]. On the other hand, a sintering method is applied to densify the shell structure by sintering temperature. The shell structure will be significantly dense in case of high temperature sintering [46]. Both of methods sometimes may lead to cause of the variation of capsule shape, capsule size and shell thickness as well as controlling of porous state. Therefore, the detail control condition is required to make a desired property of capsule. Furthermore, by considering the material to be adopted in each method, the sintering method is available for multiple materials such as metal or ceramic which can chemically retain the material structure during exposure to high temperature. While, candidate material is limited to the etching method due to chemical approach such utilizing the acid solubility.
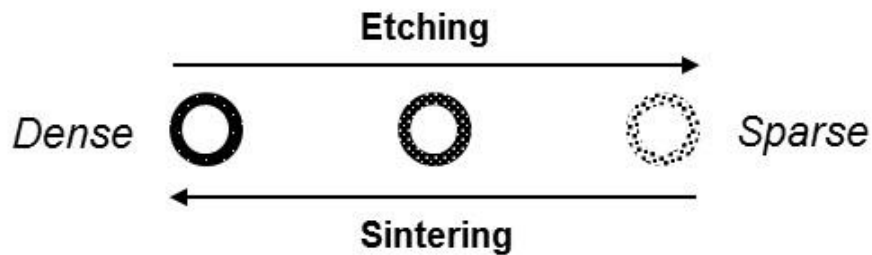
Figure 1.19 Shell structure varied by the etching and sintering

The ceramics are feasible as a matrix of the capsule shell because of high melting point with high material stability in addition to the superiority as explained above. Besides, the powder material is selected since the capsules having such shell can be obtained in a few step processes based on the powder coating process and mass

production is available, which leads to broaden the study field because of the simplicity of capsule preparation. Particularly, the shell structure can be varied with sintering process leading to design of the specific porous state for desired utilizations. In the case of sparse shell structure (open shell), the capsule is suit to apply for a selective permeation (Figure 1.20). On the contrary, the dense shell structure (closed shell) is possible to utilize as an intensive protection from external environment. It is important to know the condition for specific characteristics. However, the only intensive sintering process needs to make the closed shell. It also causes the variation of other characteristics. For example, a compressive strength of the hollow capsule made by other method in the variation of sintering temperature cannot promote simultaneously with the high porous state [46].
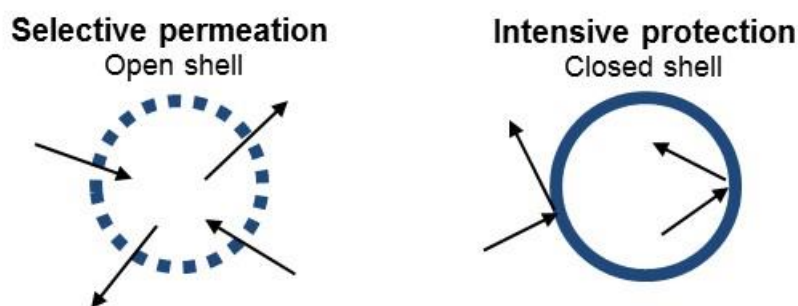
Figure 1.20 Specific utilization depended on porous state of shell structures

Instead of relying on the atomic diffusion phenomenon caused by the sintering process, the voids in open shell can be embedded by other materials (Figure 1.21). Although fine particles can generally promote the catalytic performance due to the high specific surface area, it is hard to deal with since they tend to aggregate together and adsorb other materials. Thus, such fine particles need to immobilize to overcome the inferiorities. It is close to the concept of surface modification of support materials by the catalyst to be applied in heterogeneous catalysis where the catalyst phase is different from the phase of materials to be catalyzed [17]. Furthermore, hollow capsules with the

catalytic property can be filled depending on any shapes and refilled to correspond to various conditions.
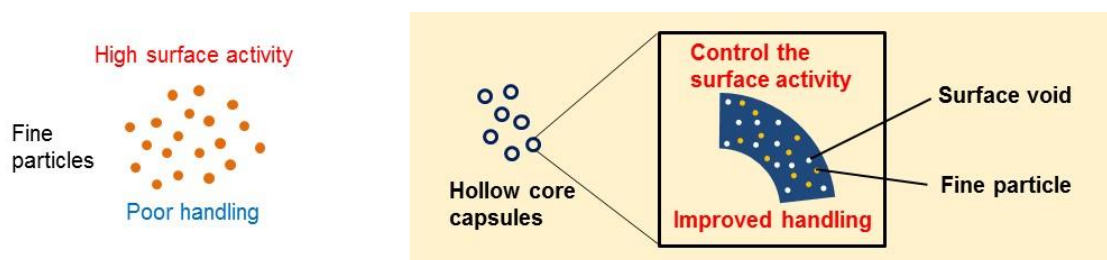
Figure 1.21 Advantage of hollow core capsules in control of the surface activity with improved handling for fine particles

To embed the voids, solution combustion synthesis (SCS) is possible to apply. SCS is a material synthesis technique to generally produce fine ceramics and starts from the solution mixture containing various metal nitrates with fuels. The high temperature condition owing to the exothermic reaction between raw materials is generated [47], thus it will not cause to promote significant sintering effect for the particles on capsule shell. It can be promising process to embed the voids on capsule shell. Among various ceramics which can be synthesized by SCS, the materials having the catalytic performance are suit to apply for the embedding material, since it is easy to evaluate the material characteristic and the geometrical characteristic of capsule with embedding materials in heterogeneous catalysis as the specific environment.

1.4 Objectives

   In the dissertation, 3 following objectives are listed to design new capsule applications involving the control of heat transfer and diffusion of liquid, and surface activity of solid by utilizing the liquid core and the hollow core capsule:

1. To elucidate the liquid and hollow core encapsulation processes and their structure controllability

2. To demonstrate the heat transfer controllability of encapsulated liquid

3. To demonstrate the material compatibility of voids embedded hollow capsules with catalysts

As for the encapsulation method, Dry water method and sacrificial template method are selected because of most simple method where the mass production in a few steps is available. In chapter 2, the heat transfer through encapsulated liquid is investigated by observing the temperature change over the encapsulated liquid. The controllability of heat transfer in liquid would help to utilize the thermal energy effectively for liquid application. In chapter 3, the effect of sintering temperature on the capsule shell structure is investigated by observing the morphology of hollow capsule. The controllability of shell structure, particularly shell porous state, would contribute to provide the specific characteristics of hollow capsule. Besides, by using a permanent magnetic material as capsule shell, it would be possible to open the application field as well as to confirm the availability of various materials which have not been used yet. In chapter 4, the effect of embedding of various catalyst candidate materials synthesized by SCS on capsule shell structure is investigated by observing the morphology of hollow capsule. The effect of type of materials is also investigated by analyzing the crystal form of materials which is exposure to methane and carbon dioxide gases flow. Because of the attractive catalysis to produce synthesis gases in recent, these gases are selected as the heterogeneous catalysis to verify the efficacy of void embedded hollow capsules with catalysts as support material. Following advantages of voids embedding by other catalyst candidate materials by SCS would be listed. Long time and high

temperature sintering is not needed during the embedding process. Fine material is immobilized for the improvement of usability. The catalytic activity can be installed to the original characteristics of hollow capsules.

References

[1] K. Bean, C. F. Black, N. Govan, P. Reynolds and M. R. Sambrook, Preparation of aqueous core/silica shell microcapsules, *J. Colloid Interface Sci.*, 366 (2012) 16-22

[2] E. Troncoso, J. M. Aguilera and D. J. McClements, Influence of particle size on the in vitro digestibility of protein-coated lipid nanoparticles, *J. Colloid Interface Sci.*, 382 (2012) 110-116

[3] M. W. Patchan, L. M. Baird, Y. R. Rhim, E. D. LaBarre, A. J. Maisano, R. M. Deacon, Z. Xia and J. J. Benkoski, Liquid-filled metal microcapsules, *ACS Appl. Mater. Interfaces,* 4 (2012) 2406-2412

[4] J. Fickert, C. Wohnhaas, A. Turshatov, K. Landfester and D. Crespy, Copolymers structures tailored for the preparation of nanocapsules, *Macromolecules* 46 (2013) 573-579

[5] Y. Yoshida and Y. Otsuka, Development of metal hollow sphere sheet and its formability and mechanical property, *Key Eng. Mater.*, Volumes 554-557 (2013) 657-663

[6] C. H. LaWall, Four thousand years of pharmacy: an outline history of pharmacy and the allied sciences, Philadelphia USA, J. B. Lippincott Company (1927)

[7] B.K. Green and L. Schleicher, Oil-containing microscopic capsules and method of making them, U. S. Patent 2,800,457, Jul. 23, 1957

[8] F. Podczeck and B. E jones, Pharmaceutical capsules, 2nd edition, London UK, Pharmaceutical Press (2004)

[9] M. Richardson and S. Stegemann, Filling two-piece hard gelatin capsules with liquids, *Tablets & Capsules*, (2007) 6 pages

[10] C. Prego, M. García, D. Torres and M. J. Alonso, Transmucosal macromolecular drug delivery, *J. Control. Release*, 101 (2005) 151-162

[11] H. Maeda, The enhanced permeability and retention (EPR) effect in tumor vasculature: the key role of tumor-selective macromolecular drug targeting, *Advan. Enzyme Regul.*, 41 (2001) 189-207

[12] B. P. Barnett, A. Arepally, P. V. Karmarkar, D. Qian, W. D. Gilson, P. Walczak, V. Howland, L. Lawler, C. Lauzon, M. Stuber, D. L. Kraitchman and J. W. M. Bulte, Magnetic resonance–guided, real-time targeted delivery and imaging of magnetocapsules immunoprotecting pancreatic islet cells, *Nature Medicine*, 13 (2007) 986-991

[13] A. Miskon, N. Ibrahim and S. N. M. Tawil, A model of defence mechanical drug delivery system (DmechD) and the drug release efficacy, *IEEE Conf. Biomed. Eng. Sci.*, (2014) 22-26

[14] F. Mohammad and N. A. Yusof, Doxorubicin-loaded magnetic gold nanoshells for a combination therapy of hyperthermia and drug delivery, *J. Colloid Interface Sci.*, 434 (2014) 89-97

[15] D. A. Hays, Paper documents via the electrostatic control of particles, J. Elecrostat., Volumes 51-52 (2001) 57-63

[16] K. Sohn, Y. J. Na, H. Chang, K. M. Roh, H. D. Jang and J. Huang, Oil absorbing graphene capsules by capillary molding, *Chem. Commun.*, 48 (2012) 5968-5970

[17] A.E. Awadallah, W. Ahmed, M.R. Noor El-Din and A. A. Aboul-Enein, Novel aluminosilicate hollow sphere as a catalyst support for methane decomposition to COx-free hydrogen production, *Appl. Surf. Sci.*, 287 (2013) 415-422

[18] J. He, Z. Liu, Y. Yoneyama, N. Nishiyama and N. Tsubaki, Multiple-functional capsule catalysts: A tailor-made confined reaction environment for the direct synthesis of middle isoparaffins from syngas, *Chem. Eur. J.*, 12 (2006) 8296-8304

[19] L. I. C. Sandberg, T. Gao, B. P. Jelle and A. Gustavsen, Synthesis of hollow silica nanospheres by sacrificial polystyrene templates for thermal insulation applications, *Adv. Mater. Sci. Eng.*, (2013) 6 pages

[20] C. S. Altamar, O. Torres, B. Teran, G. Anaya, N. A. Navarro and W. Herrera, Apparatus and process for making soft gel capsules, U. S. Patent 0049410, Mar. 1, 2012

[21] B. B. Lee, R. Ibrahim, S. Y. Chu, N. A. Zulkifli and P. Ravindra, Alginate liquid core capsule formation using the simple extrusion dripping method, *J. Polym. Eng.*, 35 (4) (2015) 311-318

[22] I. Urabe, T. Yomo, K. Yamamoto, H. Sunohara, R. Kamaguchi and Y. Hatano, Seamless capsule for synthesizing biopolymer and method for producing the same, U. S. Patent 6,251,661 Jun. 26, 2001

[23] S. Stegemann, Hard gelatin capsules today − and tomorrow, Bornem Belgium, Capsugel Belgium NV (2002)

[24] J. G. Brennan and A. S. Grandison, Food processing handbook, Weinheim Germany, Wiley-VCH (2012)

[25] A. Lewandowski, M. Czyżewski and I. Zbiciński, Morphology and microencapsulation efficiency of foamed spray-dried sunflower oil, *Chem. Eng. Process.*, 33 (1) (2012) 95-102

[26] A. Pan, H. B. Wu, L. Yu and X. W. Lou, Template-free synthesis of VO_2 hollow microspheres with various interiors and their conversion into V_2O_5 for lithium-ion batteries, *Angew. Chem.*, 125 (2013) 2282-2286

[27] P. W. Voorhees, The theory of Ostwald ripening, *J. Stat. Phys.*, 38 (1) (1985) 231-252

[28] A. A. E. Mel, R. Nakamura and C. Bittencourt, The Kirkendall effect and nanoscience: hollow nanospheres and nanotubes, Beilstein J. Nanotechnol., 6 (2015) 1348-1361

[29] R. Nakamura, D. Tokozakura, H. Nakajima, J. G. Lee and H. Mori, Hollow oxide formation by oxidation of Al and Cu nanoparticles, *J. Appl. Phys.*, 101 (7) (2007) 074303-074307

[30] H. Johnsen and R. B. Schmid, Preparation of polyurethane nanocapsules by miniemulsion polyaddition, *J. Microencapsulation*, 24 (8) (2007) 731-742

[31] P. Teeka, A. Chaiyasat and P. Chaiyasat, Preparation of poly (methyl methacrylate) microcapsule with encapsulated jasmine oil, *Energy Procedia* 56 (2014) 181-186

[32] T. Okada, S. Ozono, M. Okamoto, Y. Takeda, H. M. Minamisawa, T. Haeiwa, T. Sakai and S. Mishima, Magnetic rattle-type core–shell particles containing iron compounds with acid tolerance by dense silica, *Ind. Eng. Chem. Res.*, 53 (2014) 8759-8765

[33] F. L. Sousa, A. Almeida, A. V. Girão, S. Fateixa and T. Trindade, Multiple emulsion templating of hybrid Ag/SiO$_2$ capsules for antibacterial applications, *Part. Part. Syst. Charact.*, 32 (2015) 561-566

[34] T. Tomioka, C. Takahashi, C. Takai, M. Utsuno and M. Fuji, Effect of pH change on the shell thickness of calcium carbonate hollow particles by CO$_2$ gas bubbling method, *J. Soc. Powder Technol. Japan*, 49 (2012) 260-266 (in Japanese)

[35] T. Makuta, Y. Tamakawa and J. Endo, Hollow microspheres fabricated from instant adhesive, *Mater. Lett.*, 65 (2011) 3415-3417

[36] K. Saleh, L. Forny, P. Guigon and I. Pezron, Dry water: from physico-chemical aspects to process-related parameters, *Chem. Eng. Res. Des.,* 89 (2011) 537-544

[37] M. I. Newton, D. L. Herbertson, S. J. Elliott, N. J. Shirtcliffe and G. McHale, Electrowetting of liquid marbles, *J. Phys. D: Appl. Phys.*, 40 (2007) 20-24

[38] S. T. Gunawan, K. Kempe, G. K. Such, J. Cui, K. Liang, J. J. Richardson, A. P. R. Johnston and F. Caruso, Tuning particle biodegradation through polymer-peptide blend composition, *Biomacromolecules*, 15 (2014) 4429-4438

[39] N. Kato and N. Kato, High-yield hydrothermal synthesis of mesoporous silica hollow capsules, *Micropor. Mesopor. Mat.*, 219 (2016) 230-239

[40] W. P. Edwards, The science of sugar confectionery, The Royal Society of Chemistry, Cambridge UK (2000)

[41] R. Pfeffer, R. N. Dave, D. Wei and M. Ramlakhan, Synthesis of engineered particulates with tailored properties using dry particle coating, *Powder Technol.*, 117 (2001) 40-67

[42] C. Pfeifer, D. Kuhn and A. G. Class, Influence of injection pressure on droplet atomization and auto-ignition of dimethyl ether (DME) at elevated pressure, *Fuel*, 104 (2013) 116-127

[43] K. Shah and R. S. Besser, Understanding thermal integration issues and heat loss pathways in a planar microscale fuel processor: Demonstration of an integrated silicon microreactor-based methanol steam reformer, *Chem. Eng. J.*, 135 (2008) 46-56

[44] A. Sarı, C. Alkan, D. K. Döğüşcü and A. Biçer, Micro/nano-encapsulated n-heptadecane with polystyrene shell for latent heat thermal energy storage, *Sol. Energ. Mat. Sol. C.*, 126 (2014) 42-50

[45] W. H. Suh, A. R. Jang, Y. H. Suh and K. S. Suslick, Porous, hollow, and ball-in-ball metal oxide microspheres: preparation, endocytosis, and cytotoxicity, *Adv. Mater.*, 18 (2006) 1832-1837

[46] Z. Su, X. Xi, Y. Hu, Q. Fei, S. Yu, H. Li and J. Yang, A new Al_2O_3 porous ceramic prepared by addition of hollow spheres, *J. Porous Mater.*, 21 (5) (2014) 601-609

[47] J. J. Kingsley and K.C. Patil, A novel combustion process for the synthesis of fine particle α-alumina and related oxide materials, *Mater. Lett.*, 6 (11-12) (1988) 427-432

Chapter 2 Encapsulation of solutions for controlling heat transfer

2.1 Introduction

Liquid encapsulation is a process that covers liquid droplets by a solid shell. These covered droplets are separate the liquid from its external environment, thereby allowing easy transport and controlled release [1-3]. Particularly, interesting is the possibility of applying liquid encapsulation techniques for chemical processes where control of mass and heat transfer between capsules can produce a new type of chemical synthesis. Encapsulation of liquids produces small volumes of liquids without coalescing effects; therefore, the thermal diffusion caused by the convection and gasification in liquids during chemical synthesis can be moderated in order to use the chemical energy effectively. This concept is especially important in the field of micro scale system such as a micro reactor. However, to present knowledge, there are relatively few studies on heat transfer in powders of encapsulated liquids.

Among the various methods for the liquid encapsulation, Dry water method is possible to encapsulate a large amount of water by using a comparatively small amount of hydrophobic silica nanopowders [4]. Up to 98 wt% of water can be included in capsules by using this method [4]. Aqueous solutions containing dissolved additives also can be encapsulated if these additives do not have a significant influence on the surface tension of aqueous solutions [5]. Therefore, numerous kind of aqueous solutions are applicable to encapsulate. Besides, a capsule shell consisted of fine hydrophobic silica particles make inner solutions possible to control the dispersion rate though evaporation with varying the environmental temperature and humidity. It will lead to prevent the inner pressure from rapid increasing in capsules which causes of chemical energy lost.

In order to elucidate energy transfer between liquid capsules aiming at the effective utilization of chemical synthesis involving liquids in fine region, heat transfer

in powders consisting of capsules that include an aqueous solution prepared by Dry water method was studied in this chapter.

2.2 Experimental

2.2.1 Preparation of encapsulated solutions

Hydrophobic silica

Hydrophobic silica as the shell material of capsules with the physical properties is indicated in Table 2.1. Hydrophobic silica is surface modified with Polydimethylsiloxane to have larger water contact angle more than 90° which is categorized as hydrophobic. Water contact angle was experimentally measured an angle at which the water droplet and vapor interface meets the hydrophobic silica pellet and water droplet. The pellet was made by a pressing machine under a condition of 0.5 tons for 5 minutes.

Table 2.1 Physical properties of hydrophobic silica

Molecular formula	SiO_2 (amorphous)
Molecular weight [g/mol]	60.1
Melting temperature [K]	1,923
Ignition temperature [K]	733
Specific surface area [cm^2/g]	203
Carbon content [%]	4.5
Tap density [g/cm^3]	5.0×10^{-2}
Particle size [μm]	8.51
Water contact angle [deg.]	130
Surface modifier	Polydimethylsiloxane

Solution

The solution consisted of pure water with iodine, potassium iodide and starch was selected. It change the color from deep blue to colorless at 353 K, which is referred to as a thermochromic solution and convenient to visualize the heat transfer. Mechanism for color change is studied and explained as follows. Iodine molecule enclosed in the structure of amylodextrin as starch main composition separates from the structure due to temperature increase, resulting in the color change. It is also said that iodine is promoted to dissolve in water with the coexistence of potassium iodide. The physical properties of chemical components and weight ratio between components were described in Table 2.2. The concentration of components in pure water was about 1 wt. % which is assumed to have little influence on the surface tension of water. Iodine and potassium iodide were dissolved in a half amount of pure water, and starch was dissolved in another half amount of pure water at first, respectively. Then, both of solutions were mixed together and consequently the color change from colorless to deep blue.

Table 2.2 Physical properties of components and weight ratio in solution

	Iodine	Potassium iodide	Starch
Molecular formula	I_2	KI	$(C_6H_{10}O_5)_n$
Molecular weight [g/mol]	253.809 [6]	166.00 [6]	—
Melting temperature [K]	386.6	996	Decompose
Boiling temperature [K]	458.24	1,603	Decompose
Ratio [wt. %]	2.6	8.8	88.6

Blending condition

The mixture of hydrophobic silica and solution contained iodine, potassium iodide and starch was blended in a blender (Figure 2.1) with specifications as shown in Table 2.3. Encapsulated solutions were obtained under specific condition described in Table 2.4. To investigate the influence of ratio between hydrophobic silica and solution on heat transfer, samples contained different solution ratios were prepared.

Figure 2.1 Blender

Table 2.3 Blender specifications

| Container material	Polycarbonate
Inner volume [cm^3]	1.25×10^3
Blending speed (Low) [rpm]	15,800
Blending speed (High) [rpm]	18,500
Rated voltage [V]	100
Rated power consumption [W]	208

Table 2.4 Encapsulation conditions

Blending speed [rpm]	18,500
Blending time [s]	90
Solution ratio [wt. %]	98, 95, 90

Characterization

Morphology of encapsulated solutions contained different solution ratios were observed with an optical microscope (VHX-600, KEYENCE). The size distribution of the capsules was calculated by measuring the diameters of 100 capsules from the image of the optical microscope.

2.2.2 Temperature measurement

Figure 2.2 shows the experimental setup for the temperature measurement. The temperature of samples was measured by three thermocouples (K type), located at 5, 10 and 15 mm distances from the bottom of a glass tube. The capsule is the sphere which indicates the point contact with the thermal source; thus, the curved surface vessel in order to set the unique point of the thermal conduction was selected. It is assumed that the parallel isothermal surface in the samples starts to form from 5 mm distances from the bottom of the glass tube. Each thermocouple was connected to a data logger to record the temperature profiles. Original solution was also examined to compare with encapsulated solution. Prior to the temperature measurement, encapsulated solutions and original solution were heated at 333K for 30 min in a dry oven to obtain a vivid blue color for a clear visualization of color changes. The bottom of the glass tube was heated by using a hotplate, while the sample surface was exposed to the atmosphere. Temperature measurement was started when the glass tube touched the hotplate. Experimental conditions were also specified in Table 2.5.
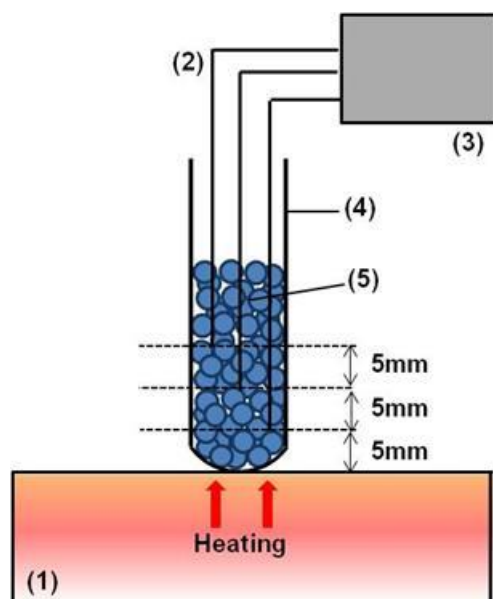
Figure 2.2 Experimental setup for the temperature measurement: (1) Hot plate, (2) Thermocouple,

(3) Data logger, (4) Glass tube and (5) Samples

**Table 2.5** Experimental condition for the temperature measurement

Sample amount [g]	1.5 (Encapsulated solution), 3.0 (Solution)
Initial temperature [K]	293
Hotplate temperature [K]	523
Measurement time interval [s]	0.5

2.3 Results and discussion

2.3.1 Morphology of encapsulated solutions

As a result of the encapsulation of the thermochromic solution, transparent capsules with wide range of droplet sizes and shapes in a form of powders were observed as shown in Figure 2.3-a1, a2 and a3. Solution droplets were completely covered with hydrophobic silica nanopowders. Some free nanopowders, which are not involved in the structure of the capsules, were found in all samples, and their amount

increased in the case of the samples with lower solution contents. According to Figure 2.3-a1, a2 and a3, the amount of hydrophobic silica nanopowders constructing each capsule membrane was approximately the same among all samples; thus, the thickness of the capsule shell is assumed to be constant. As the solution content of the samples decreased, the variance of the capsule sizes became smaller which is confirmed from Figure 2.3-b1, b2 and b3. The mean size of the capsules varied from 130 μm (90 wt%), 190 μm (95 wt%) to 230 μm (98 wt%). It can be explained such that higher solution content leads to an enlargement of the capsule sizes because of a partial coalescence of solution droplets, as a certain amount of hydrophobic silica nanopowders is needed to prevent each droplet from coalescence. The same tendency was reported by Bomhard [7].
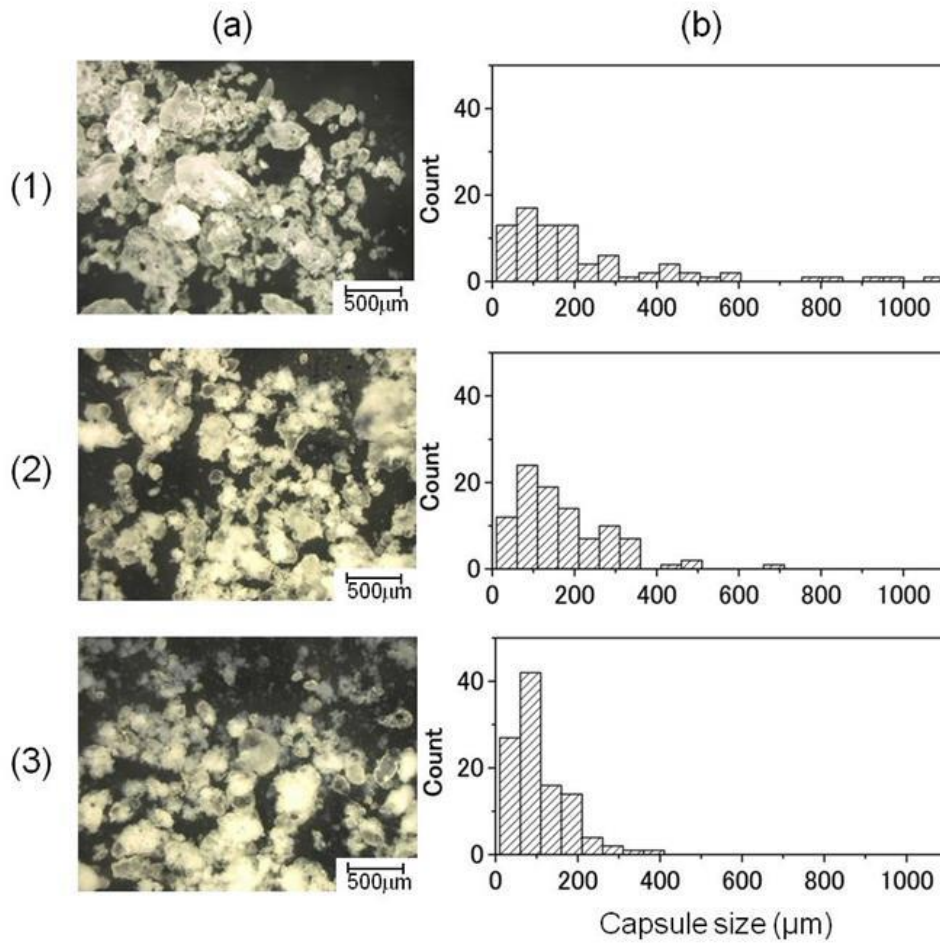
Figure 2.3 Optical microscope images (a) and size distributions of capsules (b) of encapsulated solutions for various solution contents: (1) 98 wt%, (2) 95 wt%, (3) 90 wt%

2.3.2 Observation of temperature change of encapsulated solutions

The encapsulated thermochromic solution had light blue color initially, then gradually changed their color to white from the bottom of the samples because of heating (Figure 2.4-a). A color change occurred when the temperature reached 353 K. By contrast, the color of the original solution changed uniformly in the entire volume because of the convective effect (Figure 2.4-b). Heating caused a gradual color change to yellowish after 15 min, eventually resulting in the original color of the iodine solution (which is not shown here). Hence, the process of color change is clearly different from that of the encapsulated solution.
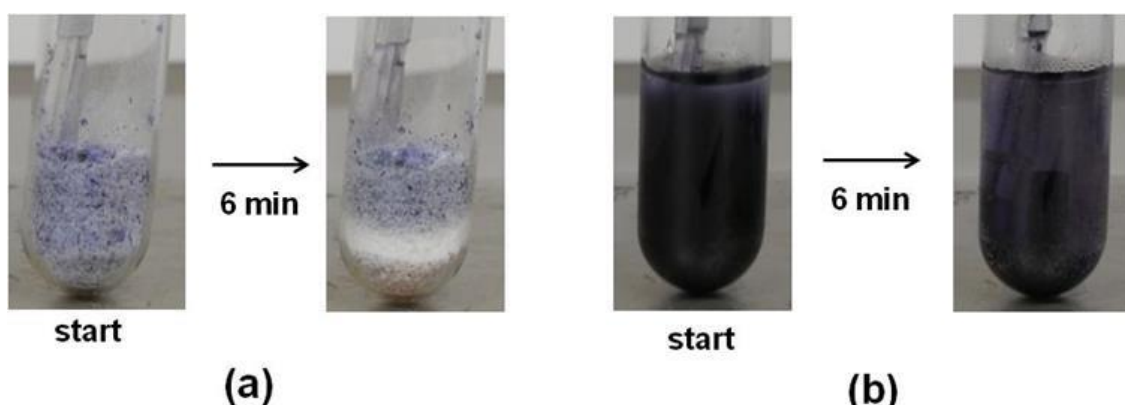
Figure 2.4 Color change images of (a) encapsulated solutions contained 98 wt % of solution and (b) original solution heated from one end

The temperature of the encapsulated solutions gradually increased to around 373K as a function of time as shown in Figure 2.5-a, b and c. Figures show that the temperature change profiles are different for each measurement point at different distances from the hot plate. This result implies that the temperature steadily increased from the bottom to the top of the samples. In contrast, the temperature of the original solution increased uniformly, which indicates that there is no significant dependency between the temperature and the measurement point (Figure 2.5-d). Thus, the liquid

flow was controlled, and the heat transfer had a particular direction in case of encapsulated solutions.
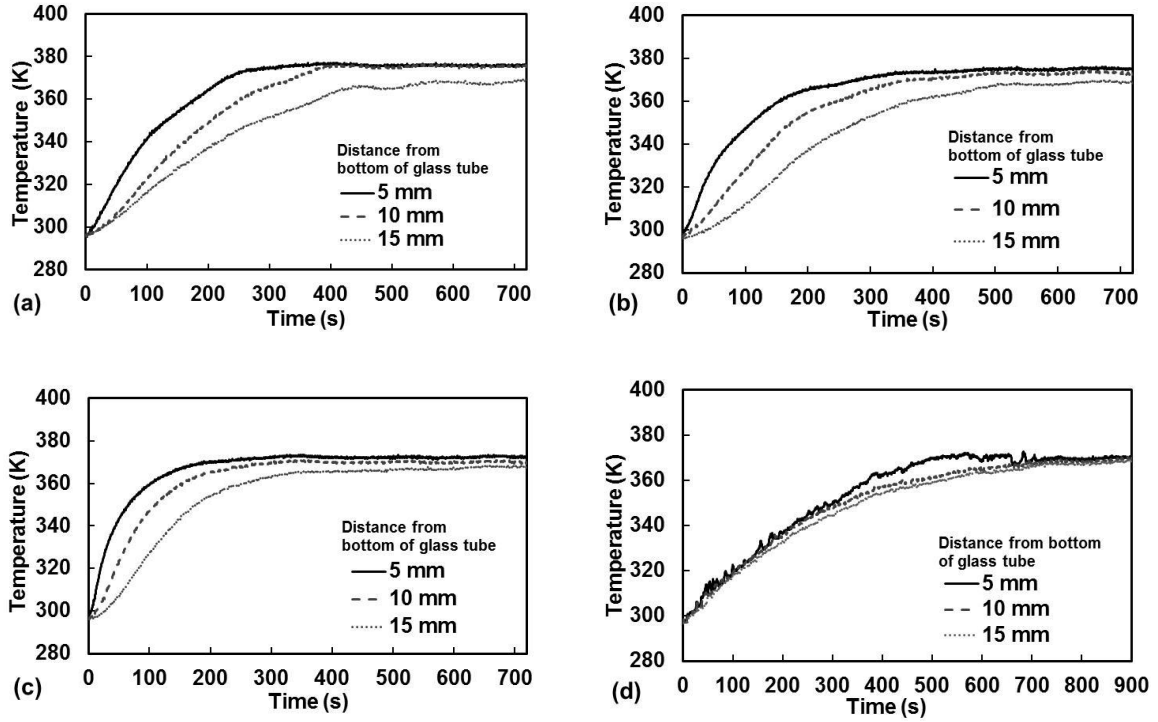
Figure 2.5 Temperature change profiles of encapsulated solutions with (a) 98, (b) 95 and (c) 90 wt % solution contents and (d) original solution

Figure 2.5 shows that the temperature exponentially changed and differed depending on the solution contents and distance from the hot plate. Based on the data of each measurement point shown in Figure 2.5, a rate constant, k (/s), was calculated as follows when the temperature of each sample increased until an equilibrium temperature from initial temperature:

$$k = - \log ((T_{eq} - T_{(t)})/(T_{eq} - T_i)) / t \tag{1}$$

where $T_{(t)}$ (K) is a temperature when specific time has elapsed since the measurement started, T_{eq} (K) is an equilibrium temperature, T_i (K) is the initial temperature and t (s) is the elapsed time.

The equation (1) was based on Newton's law of cooling and derived from equation (2) as follows:

$$T_{(t)} = T_{eq} - (T_{eq} - T_i) \exp(-kt) \tag{2}$$

The calculated values of k for the original solution and encapsulated solutions with 90, 95 and 98 wt% solution contents are shown in Figure 2.6.
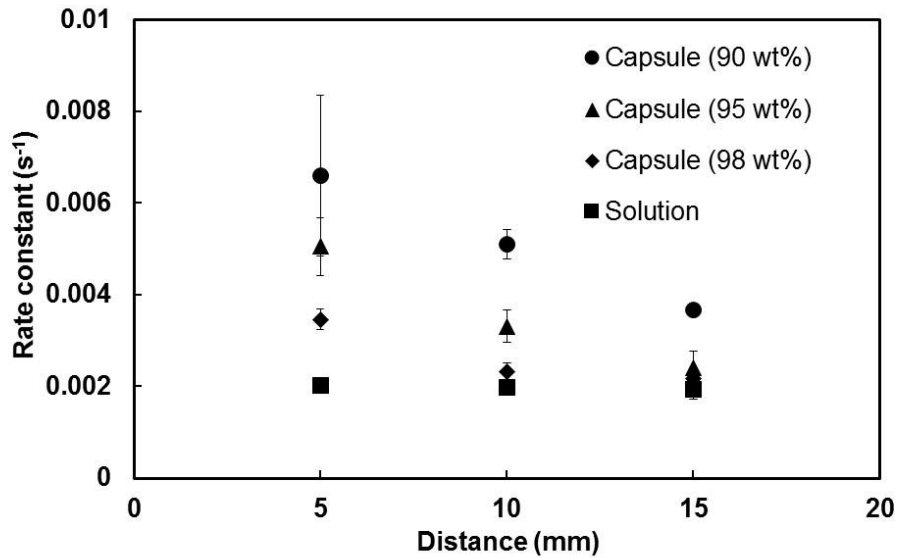
Figure 2.6 Rate constant of original solution and encapsulated solutions contained 98, 95 and 90 wt % of solution at each measurement point from the bottom of glass tube

There was no significant difference between each measurement point for original solution. This means that the temperature increased uniformly in the entire volume because of the convective effect. The rate constant for powders of encapsulated solutions was higher than that of the original solution and decreased with the distance from the bottom of the glass tube increases. The figure also shows that the values for the encapsulated solutions were dependent on the solution contents. The rate constant of

39

lower solution contents was larger compared with that of higher solution contents, which indicates that heat transfer was faster in the case of lower solution contents. A large distribution shown at short distance from the bottom of the glass tube for lower solution contents would be caused by experimental error.

The composition of all encapsulated solutions samples is dominated by water; thus, it can be assumed that the thermal behavior of samples is mainly determined by the thermal property of water. Among all components, the highest thermal conductivity (0.6 W/m·K [6]) and specific heat (4.2 J/g·K [6]) values belong to water. According to the results, the temperature increased faster in the case of samples with lower solution contents. However, there is a limiting factor for the temperature increase of samples with different solution contents. In the case of the sample with 90 wt% solution content, the total amount of water and size of capsules are smaller compared to the sample with 98 wt% solution content. The amount of heat energy that is necessary to increase the temperature for a single capsule from 293 K (room temperature) to 353 K can be estimated by a calorific calculation. The volume of the capsule and the mass of water were calculated by using an average diameter of the capsules; on the assumption that capsule shape is an ideal sphere. The thickness of the capsule shell was regarded to be 10 μm in all samples. The heat energy of a single capsule Q [J] was calculated by using the following equation:

$$Q = M \, C_p \, \Delta T \tag{3}$$

where M (g) is the mass of a capsule, C_p(J/g·K) is the specific heat of a capsule, and ΔT (K) is a temperature gradient (60 K in this case).

Here, the mass of a capsule was estimated by using experimental data with densities of water (1 g/cm^3 [6]) and silica (0.05 g/cm^3, tapped density determined experimentally). The specific heat of a capsule was calculated by using the data for water (4.2 J/g·K [6]) and silica (0.85 J/g·K [8]). Therefore, the number of capsules in a unit volume was

estimated. To simplify the calculation, no free hydrophobic silica nanopowders are existed, which means that all of them are assumed to be involved in the capsule shell. Furthermore, considering the heat transfer of encapsulated solutions, only thermal conduction can be taken into account in this calculation. As a result, the total heat energy necessary to increase the temperature of a unit volume for each sample from 293 K to 353 K was calculated. In the calculation, the air included in the samples was also considered. Table 2.6 shows the lowest values of heat energy in a unit volume of a sample with 90 wt. % solution content among all samples. The time needed to increase the temperature is shortened in the case of samples with lower solution contents. The calorific calculation is adequate to describe the difference between samples observed in the experiments.

Table 2.6 The data for calorific calculation of encapsulated solutions

Solution content (wt%)	98	95	90
Average diameter (µm)	230	190	130
Mass of capsule (µg)	4.92	2.62	0.719
Volume of capsule (µm^3)	6.37×10^6	3.59×10^6	1.15×10^6
Number of capsules (cm^{-3})	1.38×10^5	2.06×10^5	5.25×10^5
Heat energy of capsule (mJ)	1.23	0.651	0.177
Heat energy (J·cm^{-3})	169	134	93

2.4 Conclusions

Observation of temperature change though encapsulated iodine-starch (thermochromic) solutions with different solution contents prepared by dry water method was studied. The encapsulated solutions were possible to control the convective effect in liquids and exhibited the particular direction of temperature change. The temperature in samples with lower solution contents rises faster compared with the temperature in higher solution content samples. This effect can be explained by the

calculation of heat energy based on the difference in packing densities and capsule sizes among the samples with different solution contents. The results suggest that it is possible to control the propagation speed of heat by varying the content of the encapsulated solutions.

References

[1] L. Han, L. Bi, Z. Zhao, G. Gao and Y. Xing, Preparation and characterization of microcapsules containing squalene, *Bioenerg. Res.*, (2013) 1-9

[2] R. Luo,S. S. Venkatraman and B.Neu, Layer-by-layer polyelectrolyte−polyester hybrid microcapsules for encapsulation and delivery of hydrophobic drugs, *Biomacromolecules*,14 (2013) 2262-2271

[3] A. Abbaspourrad, N. J. Carroll, S.-H. Kim and D. A. Weitz, Polymer Microcapsules with Programmable Active Release, *J. Am. Chem. Soc.*,135 (2013) 7744−7750

[4] K. Saleh, L. Forny, P. Guigon and I. Pezron, Dry water: from physico-chemical aspects to process-related parameters, *Chem. Eng. Res. Des.,* 89 (2011) 537-544

[5] L.Forny, K. Saleh, I.Pezron, L.Komunjer and P.Guigon, Influence of mixing characteristics for water encapsulation by self-assembling hydrophobic silica nanoparticles, *Powder Technol.,*189 (2009) 263-269

[6] J. A. Dean, Lange's handbook of chemistry fifteenth edition, McGRAW-HILL, INC. (1999）

[7] J. Bomhard, Dry Water, Master's Thesis, Luleå University of Technology, Sweden, (2011）

[8] H. Simmler, S. Brunner, U. Heinemann, H. Schwab, K. Kumaran, P. Mukhopadhyaya, D. Quénard, H. Sallée, K. Noller, E. Kücükpinar-Niarchos, C. Stramm, M.Tenpierik, H.Cauberg, and M. Erb,Vacuum Insulation Panels. Study on VIP-components and Panels for Service Life Prediction ofVIP in Building Applications (Subtask A), IEA/ECBCS Annex 39 High Performance Thermal Insulation, (2005)

Chapter 3 Effect of sintering temperature on the characteristics of hollow capsules produced by sacrificial template method

3.1 Introduction

Hollow capsules have gained an attention because they have various potential advantages involving improvement of adsorptivity, permeability and insulation properties. Hollow capsules can serve as primary units for cellular or macroporous composite with filling ratio controllability and flexible shape selectivity. The presence of inner hollow space can be a useful property for a thermal insulation material due to its low thermal conductivity [1, 2]. The key characteristics of hollow capsules, which will determine their functionality, are structural properties such as a sphere size, a shell thickness and porosity of the shell as well as physicochemical properties of the shell material. Particularly, the porosity of the shell structure is an important characteristic due to its influence on mechanical integrity of the hollow capsules and their functional properties such as permeability. In general, the porosity of porous materials is defined as a void fraction in material. When numerous fine voids remain in the shell, high porosity can be attained. High void fraction is effective for promotion of catalytic activity due to an increase in specific surface area [3, 4]. In case of ceramics, the size of void and void fraction can be controlled irreversibly by a sintering process. Due to high melting points and high material stability of ceramics, a wide range of sintering conditions is available.

To prepare the hollow capsules, the sacrificial template method with powder coating process was selected. The sacrificial template method [5] is based on dissolution or pyrolysis of a core material covered by raw materials of the hollow capsules which results in formation of shell. The formation process can be controlled by characteristics of precursor and template removal conditions. Particularly, combination of solid organic core material and ceramic powder is attractive for industrial field since a mass production is highly possible in a few steps with variable control conditions and flexible material selectivity [6-9]. The concept of this technique is similar to fabrication method

for a foamed body [10] which is also enable to use as the porous material. The inner hollow space in hollow capsule is more homogeneously produced compared with that in foamed body due to the individual designed process [11]. However, from the scientific point of view, fabrication of the hollow capsules by this technique has not been investigated in detail. In this chapter, the effect of sintering temperatures on the structural properties of the hollow capsules such as a sphere diameter, shell thickness, void diameter between sintered powder particles, specific surface area and total pore volume was investigated. As a material for hollow capsules, strontium ferrite ($SrFe_{12}O_{19}$) was selected due to its permanent magnetic property which is attractive for applications in various fields.

3.2 Experimental

3.2.1 Preparation of hollow capsules

Materials

Component materials used for the preparation of hollow capsules' precursor are described in Table 3.1. Polyvinyl alcohol (PVA) with a saponification degree of more than 78 % was selected as a binder with water soluble property. The binder is a key factor to retain the hollow spherical structure. Strontium ferrite powder with an average particle diameter and standard deviation of 2 ± 1 μm, bulk density of 2.3 g/cm^3 was used as a matrix of hollow capsules. Expanded polystyrene (EPS) beads with an average diameter and standard deviation of 870 ± 95 μm, bulk density of 0.6 g/cm^3 and weight-average molecular weight of more than 300,000 was selected as a sacrificial template with spherical shape. Size difference between strontium ferrite powder and EPS is enough to achieve the ordered mixing. All of organic materials have a pyrolysis temperature less than 773 K.

Material	Polyvinyl alcohol	Strontium ferrite	Expanded polystyrene
Molecular formula	$+CH_2-CH+_{1,600} +CH_2-CH+_{400}$ $\quad\quad OH \quad\quad\quad OCOCH_3$	$SrFe_{12}O_{19}$	
Molecular weight [g/mol]	104,800	1,062	>300,000
Melting temperature [K]	< 773 (Pyrolysis)	> 1,643	<773(Pyrolysis)

Preparation procedure

Preparation of hollow capsules is consisted of 2 processes: Coating process and heating process. Firstly, 1 wt .% PVA was put in pure water and the solution mixture was left for 2 hours to obtain well-dissolved solution. Secondly, the strontium ferrite powders were added to the solution. The solution mixture was placed in a dry oven heated at $60\,^{\circ}C$ for 6 hours and stirred for several seconds every one hour. After the drying, the solution became a solid mixture. Thirdly, the solid mixture was milled for 30 minutes until it got powder state using a vibratory ball mill (SPARTAN, FRITSCH) under vertical vibration at 3,000 times per minutes. Milling medium was a stainless steel ball with diameter of 5 cm and weight of 500 g. Lastly, EPS the mixture powders were put in the blender which is described in 2.2.1. A weight ratio of strontium ferrite powder, EPS and PVA in the coated precursors was 93, 5 and 2. The mixture was blended for 2 minutes with blade speed of 1,200 round per minutes. Distilled water (5 wt. % of the total weight of all components) was added dropwise in the blender during the blending. To obtain homogeneous coated precursors, the blending process was repeated again under the same conditions described above. Prior to the blending process, the blender geometrical condition was modified. The surrounding of blender's blade was covered by a Teflon sheet with inner diameter of 6 cm and height of 14.5 cm.

Besides, a steel wire was connected with the blade. Each edge of wire was extended to along the inner side of the Teflon sheet and a bottom surface under the blade, respectively. The bottom surface was raised with an epoxy resin adhesive to near an edge of blade as much as possible. The purpose of this modification was to decrease a dead space where the mixture is stagnated.

And then, coated precursors were placed in a programmed furnace (NHK-170, NITTO KAGAKU Co., Ltd.) under the heating condition as visually described in Figure 3.1. Firstly, the temperature was increased from room temperature to 773 K at the rate of 4 K / min. and kept at 773 K for 1 hour to complete pyrolysis of organic components. Secondly, the temperature was increased to higher temperature at the rate of 10 K / min. and was kept at specific sintering temperature. Thereafter, the sample was cooled naturally in the furnace. The sintering temperatures were set at 1,373 K, 1,423 K, 1,473 K and 1,523 K. All of steps mentioned here were conducted under an atmospheric condition.
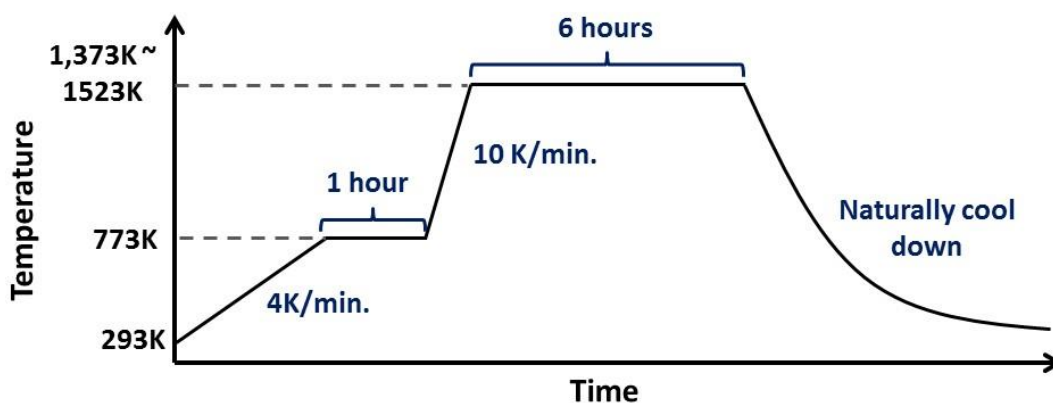
Figure 3.1 Temperature profile for coated precursor heating

3.2.2 Characterization

The diameter of hollow capsules and thickness of their shell sintered at each temperature were measured by using an optical microscope (VHX-600, KEYENCE). To measure the shell thickness, the hollow capsules were embedded in an epoxy resin

adhesive and were cut at the area contained hollow capsules after the resin was hardened. The void area ratio, defined as a sum of void areas on the shell surface divided by a total surface area, was calculated from scanning electron microscope (SEM, JSM-6610LA, JEOL) images. Here, the void was assumed to have a spherical shape and the diameter of void was approximately defined in a range from a few hundred nanometers to few micrometers. The specific surface area of hollow capsules sintered at each temperature was calculated by Brunauer–Emmett–Teller (BET) method based on nitrogen gas adsorption (BELSORP-28SA, MicrotracBEL Corp.) at 77 K. The total pore volume was calculated from a maximum adsorbed amount of nitrogen. Prior to the nitrogen adsorption analysis, all samples were dried at 333 K for 24 hours and heated at 573 K for 200 min to remove adsorbed gases from the surface. BET equation (4) is used to derive an equation (5) for the calculation of specific surface area. The total pore volume can be calculated from maximum amount of adsorbed nitrogen which is defined as equation (6). Besides, it is assumed that the pores on the surface are filled with liquid nitrogen.

$$V = \frac{V_m C p}{(p_0 - p)(1 + (C-1)(p/p_0))}$$ (4)

where V is amount of adsorbed nitrogen (m^3/g), V_m is amount of adsorbed nitrogen on monolayer (m^3/g), C is constant, p is equilibrium pressure (Pa) and p_0 is saturated vapor pressure (Pa). Here, the constant C expresses how the nitrogen interacts with the surface. Strong interaction between them would be indicated if this value is considerable higher than 1.

$$S = \frac{V_m N a_m}{M}$$ (5)

where S is specific surface area (m^2/g), V_m is amount of adsorbed nitrogen on monolayer (m^3/g), N is Avogadro constant (/mol), a_m is molecular occupied cross-sectional area (m^2) and M is molecular weight of nitrogen (g/mol)

$$Vp = \frac{P_a V_{max} V_l}{RT}$$ (6)

where V_p is total pore volume (m^3/g), P_a is ambient pressure (Pa), V_{max} is maximum amount of adsorbed nitrogen (m^3/g), V_1 is molar volume of liquid nitrogen (m^3/mol), R is gas constant (Pa m^3/mol/K) and T is ambient temperature (K)

3.3 Results and discussion

3.3.1 Shape of hollow capsules

Figure 3.2-a shows optical photographs of hollow capsules sintered at 1,373 K. Average roundness of the hollow capsules defined as a ratio between the diameters of the inscribed and circumscribed circles fitting the shape of a hollow capsule was around 90 % for all samples. It can be said that all samples retained the original spherical form because their roundness was similar to the roundness of EPS. However, the average diameter decreased as the sintering temperature increases as shown in Figure 3.3. There is 14 % difference between the average diameters of hollow capsules sintered at 1,373 K and 1,523 K. The result shows that rising the sintering temperature significantly promoted a size shrinking of hollow capsules. As a result, the average diameter of hollow capsules became less than that of EPS. According to a preliminary experiment, the organic components were thermally decomposed at temperature less than 773 K while the hollow spherical shape retained. Figure 3.2-b shows a cross-sectional view of single hollow capsule. The variation of average shell thicknesses between the hollow capsules sintered at 1,373 K and 1,523 K was 18 % which can be seen from Figure 3.3. The shell thickness for all samples also had the standard deviation due to a nonhomogeneous coating during the precursor preparation. From average diameters and thicknesses, a core volume ratio which is a ratio between core volume and total volume was calculated for each sample. All of samples had core volume ratios of around 75 %. The decreasing of thickness which was coincident with the size shrinking caused no significant variation of core volume ratio among samples.
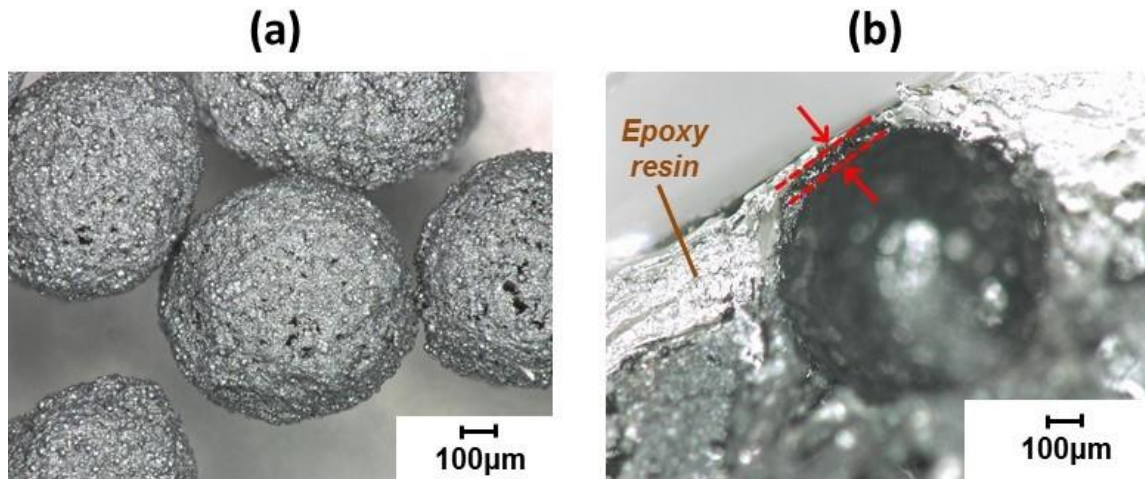
Figure 3.2 Hollow capsules sintered at 1,373 K (a) and its cross-section (Shell thickness shown as the width of red dotted line) (b).
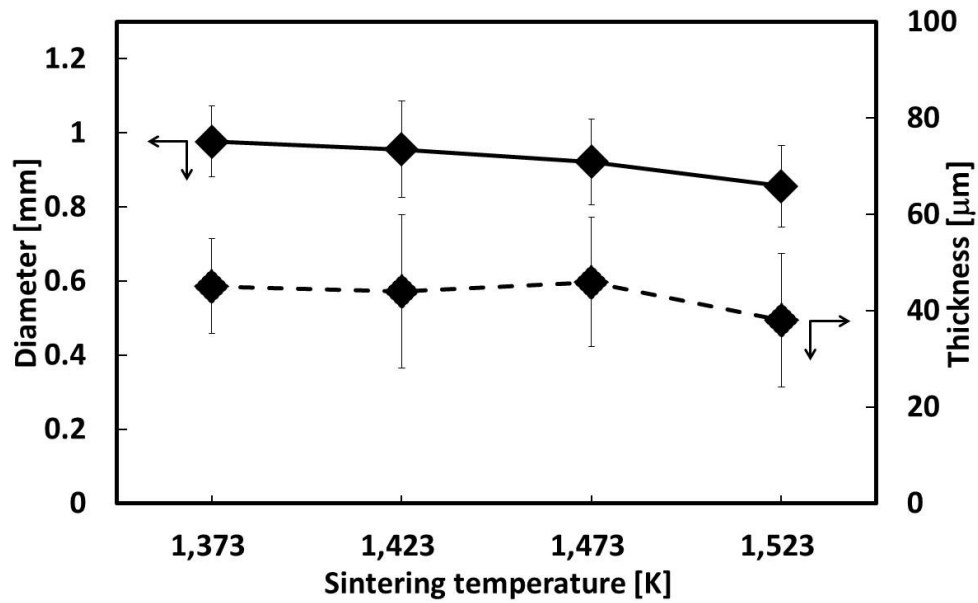

Figure 3.3 Diameter (solid line) and shell thickness (dotted line) of hollow capsules sintered at each temperature.

3.3.2 Shell surface morphology

Figure 3.4 shows surface images of hollow capsules sintered at each temperature which was observed by SEM. Hexagonal particles shown in Figure

represent a typical crystal form of $SrFe_{12}O_{19}$ [12, 13]; the particle size growth was promoted with increasing the sintering temperature. It is also confirmed that numerous voids existed between the particles. The voids can mainly appear during the coating process. As the sintering temperature increases, number of voids tends to decrease (Figure 3.4). It can be seen from the figure, that by increasing sintering temperature from 1,373 K to 1,523K, void area ratio decreased by 9.2 times as shown in Figure 3.5. Since the particle size growth and necking of particles were promoted as the sintering temperature increases, the size of a few micrometers voids would be decreased to submicron size. However, such fine scale void could not clearly distinguished from SEM observation because the particle size and necking state were sterically grew which was corresponded to the result of the shrinking of shell structure.
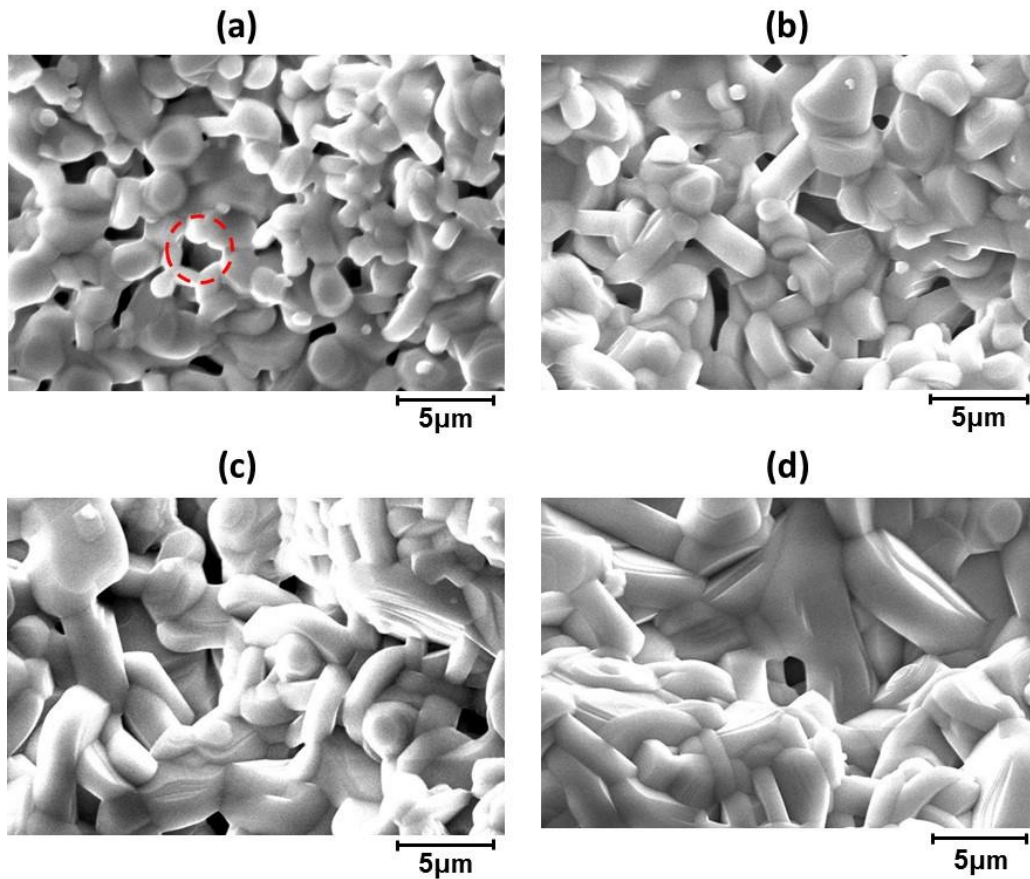
Figure 3.4 Surface images of hollow capsules sintered at 1,373 K (a), 1,423 K (b), 1,473 K (c) and 1,523 K (d) (The red dotted circle indicates the void)
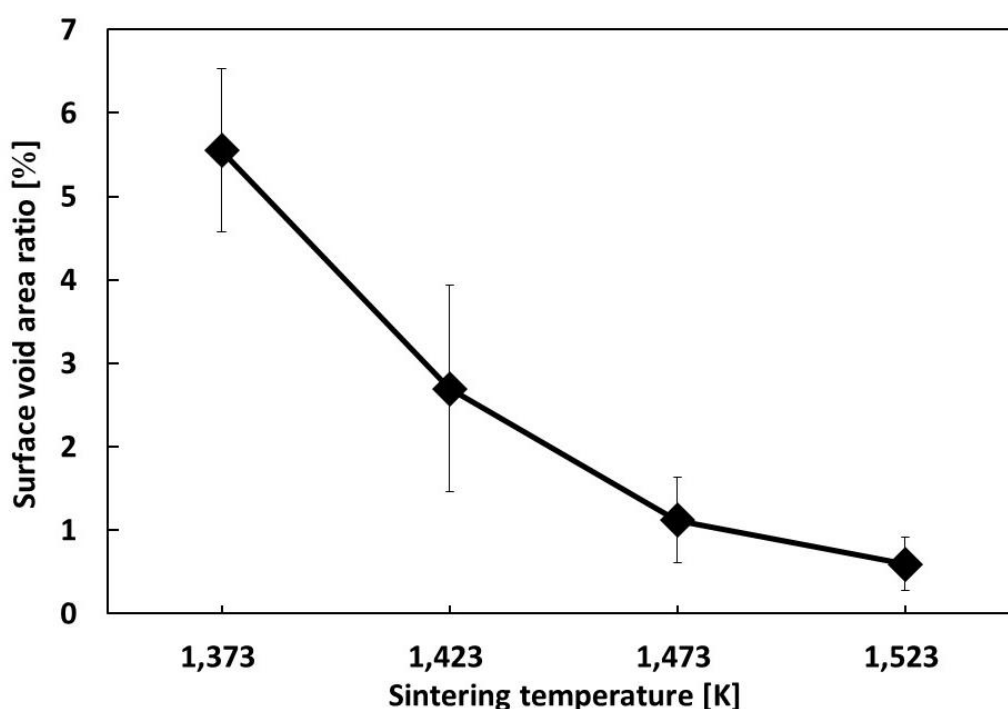
Figure 3.5 Surface void area ratio based on the observation of surface images of hollow capsules sintered at each temperature.

3.3.3 Gas adsorption property

Figure 3.6 shows the adsorption isotherm for the hollow capsules sintered at each temperature. Each isotherm is defined as the relationship between the amount of adsorbed nitrogen per unit mass and the equilibrium relative pressure. Besides, the shape of isotherms can belong to the Type II according to the classification issued by IUPAC [14]. This type is generally characteristic for non-porous or macroporous solids and is often obtained in the case of nitrogen adsorption on iron or oxide surface [15]. A hysteresis between adsorption and desorption curves observed for all samples could be caused by an insufficient time for the gas desorption. Because, the surface of hollow capsules significantly interact with nitrogen molecules. From Figure 3.6, it can be seen that the maximum adsorbed amount decreased as the sintering temperature increases. There was approximately 1.6 times difference in the maximum adsorbed amounts of nitrogen between the sample sintered at 1,373 K and that sintered at 1,523 K. By

51

calculating from the adsorption data, the BET specific surface area and total pore volume became smaller with increasing the sintering temperature as shown in Table 3.2. It can be concluded that higher sintering temperature intensively promoted closing of pores inside particles and voids between them in the shell of hollow capsules. However, the obtained values of specific surface area for all samples were still quite high and can be corresponded to that hundreds nanometer size particles exist in the shell according to simple estimation. Therefore, even sintered at higher temperature hollow capsules with high specific surface area could be designed.
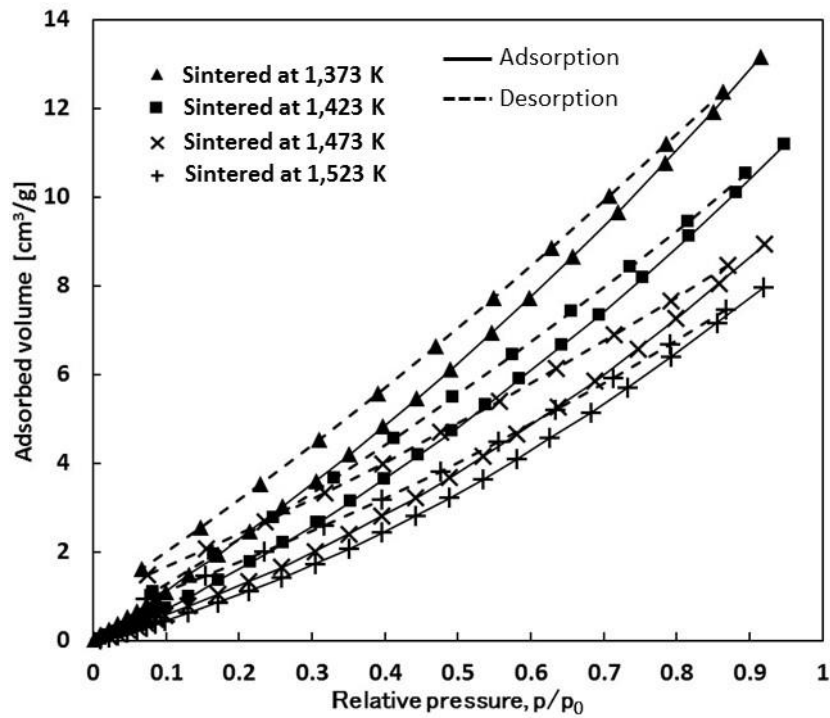
Figure 3.6 Nitrogen adsorption and desorption isotherm curves of hollow capsules sintered at each temperature.

Table.3.2 Specific surface area and total pore volume of hollow capsules sintered at each temperature.

Sintering temperature [K]	Specific surface area [m²/g]	Total pore volume [cm³/g]
1,373	22.8	0.020
1,423	20.2	0.017
1,473	13.8	0.014
1,523	14.3	0.012

3.4 Conclusions

The structure of hollow capsules prepared by the sacrificial template method and sintered at different temperatures was studied by the microscopic observation and the gas adsorption test. With increasing the sintering temperature, the diameter of hollow capsules, shell thickness, void area ratio on the shell, specific surface area and total pore volume decreased. The result revealed that the shrinking of hollow capsules, decreasing number of voids in the shell and closing of pores in powder particles were significantly promoted with increasing the sintering temperature. To sum up, the structure of hollow capsules could be controlled carefully with the sintering temperature.

References

[1] A. Cha´vez-Valdez, A. Arizmendi-Morquecho, G. Vargas, J.M. Almanza and J. Alvarez-Quintana, Ultra-low thermal conductivity thermal barrier coatings from recycled fly-ash cenospheres, *Acta Mater.*, 59 (2011) 2556-2562

[2] P. Ruckdeschel, T. W. Kemnitzer, F. A. Nutz, J. Senkerb and M. Retsch, Hollow silica sphere colloidal crystals: insights into calcination dependent thermal transport, *Nanoscale*, 7 (2015) 10059–10070

[3] J. Sun, C. Xing, H. Xu, F. Meng, Y. Yoneyama and N. Tsubaki, Filter and buffer-pot confinement effect of hollow sphere catalyst for promoted activity and enhanced selectivity, *J. Mater. Chem. A*, 1 (2013) 5670-5678

[4] Y. Yamada, M. Mizutani, T. Nakamura and K. Yano, Mesoporous microcapsules with decorated inner surface: fabrication and photocatalytic activity, *Chem. Mater.*, 22 (2010) 1695-1703

[5] L. I. C. Sandberg, T. Gao, B. P. Jelle and A. Gustavsen, Synthesis of hollow silica nanospheres by sacrificial polystyrene templates for thermal insulation applications, *Adv. Mater. Sci. Eng.*, (2013) 6 pages

[6] Y. Fukuda, L. Weiping and K. Ogura, Fabrication of iron hollow spheres by reduction processing process, *J. Jpn. Soc. Powder Powder Metall.*, 58 (2) (2010) 134-138

[7] T. Kato, Method for producing ferrite hollow particles, U. S. Patent 7,105,144, Sep. 12, 2006

[8] M. Jaeckel and H. Smigilski, Process for producing metallic or ceramic hollow-sphere bodies, U. S. Patent 4,917,857, Apr. 17, 1990

[9] O. Andersen, U. Waag, L. Schneider, G. Stephani and B. Kieback, Novel metallic hollow sphere structures, *Adv. Eng. Mater.*, 2 (4) (2000) 192-195

[10] N. Inoguchi, M. Kobashi and N. Kanetake, Synthesis of porous Al3Ti/Al composite and effect of precursor processing condition on cell morphology, *Mater. Trans.*, 50 (11) (2009) 2609-2614

[11] J. K. Cochran, Ceramic hollow spheres and their applications, *Curr. Opin. Solid State Mater. Sci.*, 3 (1998) 474-479

[12] N. Langhof, D. Seifert, M.Göbbels and J.Töpfer, Reinvestigation of the Fe-rich part of the pseudo-binary system SrO–Fe$_2$O$_3$, *J. Solid State Chem.*, 182 (2009) 2409-2416

[13] M. M. Rashad and I. A. Ibrahim, A novel approach for synthesis of M-type hexaferrites nanopowders via the co-precipitation method, *J. Mater. Sci: Mater. Electron.*, 22 (2011) 1796-1803

[14] K. S. W. Sing, D. H. Everette, R. A. W. Haul, L. Moscou, R. A. Pierotti, J. Rouquerol and T. Siemieniewska, Reporting physisorption data for gas/solid systems with special reference to the determination of surface area and porosity, *Pure & Appl. Chem.*, 57 (4) (1985) 603-619

[15] F. V. Molina, Soil colloids: properties and ion binding, CRC Press, Boca Raton USA (2013)

Chapter 4 Material compatibility of voids embedded hollow capsule under methane and carbon dioxide gases flow condition

4.1 Introduction

The controllability of shell structure of hollow capsule was elucidated in terms of the temperature in the sintering process as described in Chapter 3. As the result of present study, the densification of shell structure due to intensive sintering caused the decreasing of void area ratio on the shell surface and specific surface area or total pore volume of hollow capsule. Simultaneously, the hollow capsule diameter and shell thickness decreased. In other words, the result indicated that each parameter cannot be varied independently with various sintering temperatures. This is not only a natural consequence but also a practical issue which would cause an industrial inferiority, therefore, an elaboration to obtain the hollow capsule with specific parameters should be explored.

In this chapter, a new embedding technique where other materials embed the pores and voids in the shell was developed. The embedding material compatibility with the material of hollow capsule under specific environment was studied. By introducing the other materials instead of high temperature sintering to hollow capsule, the pore and void spaces are possible to utilize as well as a controlling of porous state. To embed the pores and voids, a solution combustion synthesis (SCS) technique was selected. SCS is a synthesis method where fine solid powder up to nano scale size can be produced through a redox reaction in raw material mixture solutions containing metal nitrates with fuels such as urea or glycine [1, 2]. The fine size is caused by that raw materials are dissolved in the solution in molecular level and a dispersion of gas bi-products decomposed from organic components inhibits the particle size growth [2]. The high reaction temperature over 1,173 K during the combustion is generally occurred within several seconds [2]. This feature would not make a long time high temperature condition which causes the promotion of sintering. Besides, tremendous variations of

materials involving oxide, metal and their composite have been reported by means of SCS. As for the embedding material, non-precious metal nitrates were selected as the raw materials of oxides which can be prospective for the mass production.

To elucidate the compatibility between embedding material and hollow capsule material is also important to make sure a stability of the crystal form as well as the morphology under specific environments. It is due to that the hollow capsules would be exposure to extraordinary environments such as high temperature, high pressure, acidic environment or rapid stream fluid environment which are dependent on the utilization. In order to evaluate the compatibility, the shell surface modified capsule was exposure to heating and gas flowing condition. The gases consisting of the methane, carbon dioxide and nitrogen was selected. The methane and carbon dioxide with a coexistence of transition metals or noble metals at the temperature from 1,073 K to 1,273 K can convert to a hydrogen and carbon monoxide which is also known as a dry reforming of methane [3]. This is the heterogeneous catalysis and has been attracted in the scientific and industrial field over the last few years owing to an effective utilization of green-house gases converting to synthesis gases [4]. Besides, the spinel form produced by SCS with other oxides has been considered as a prospective material which can promote a catalytic activation [5]. Therefore, this technique would be expected to be a new utilization of hollow capsule prepared by the sacrificial template method.

4.2 Experimental

4.2.1 Preparation of shell structure modified hollow capsule

Materials

In order to investigate various material compatibilities, multiple raw materials were selected. The physical properties of metal nitrates and urea used as raw materials for shell structure modification of hollow capsule were described in Table 4.1 and 4.2. All of raw materials here are soluble in water and most of them will start to decompose at less than 700 K.

Table 4.1 Physical properties of metal (nickel, cobalt and cerium) nitrates [6]

	Nickel (II) nitrate hexahydrate	Cobalt (II) nitrate	Cerium (III) nitrate hexahydrate
Molecular formula	$Ni(NO_3)_2\ 6H_2O$	$Co(NO_3)_2$	$Ce(NO_3)_3\ 6H_2O$
Molecular weight [g/mol]	290.79	244.948 [7]	434.23
Melting temperature [K]	329.7	—	150 (Change to trihydrate)
Decomposition temperature [K]	409.7 (Boiling)	448 [8]	473

Table 4.2 Physical properties of metal (magnesium, aluminium and iron) nitrates and urea [6]

	Magnesium (II) nitrate hexahydrate	Aluminium (III) nitrate hexahydrate	Iron (III) nitrate hexahydrate	Urea
Molecular formula	$Mg(NO_3)_2\ 6H_2O$	$Al(NO_3)_3\ 9H_2O$	$Fe(NO_3)_3\ 9H_2O$	$CO(NH_2)_2$
Molecular weight [g/mol]	256.41	375.13	404	60.06
Melting temperature [K]	362	346.5	320.2	—
Decomposition temperature [K]	603	423	398	408

Preparation procedure

Firstly, metal nitrates, urea and Polyvinyl alcohol (PVA) were dissolved in a pure water of a glass beaker with specific ratios as listed in Table 4.3. PVA with same physical property specified in Table 3.1 was added as a binding agent. After stirring the solution for several seconds, hollow capsule prepared by same process as described in 3.2.1 were impregnated in the solution with a ratio described in the Table 4.3. The hollow capsule used here was sintered at 1,373 K which had large porous state. The solution containing hollow capsules was also stirred for several seconds. A part of raw material molecules in the solution were considered to be pass through the voids in the shell into the inner core space of hollow capsule. Secondly, the mixture was put in a furnace heated at 773 K for 10 minutes. SCS process was completed within the time. Lastly, the glass beaker containing the mixture was removed from the furnace and placed on an alumina brick to cool naturally to room temperature. Finally, the shell structure modified hollow capsules were prepared. All of steps were conducted in the atmospheric condition and visually shown in Figure 4.1. 6 samples were prepared with different metal nitrates compositions and classified in 2 types: Ni-Co-O based sample and Mg-Al-Fe-O based sample as described in Table 4.4. In addition, some samples included additives such as Ce, Mg, Al or Co. The weight ratio of each sample was based on empirical results to synthesis spinel structure.
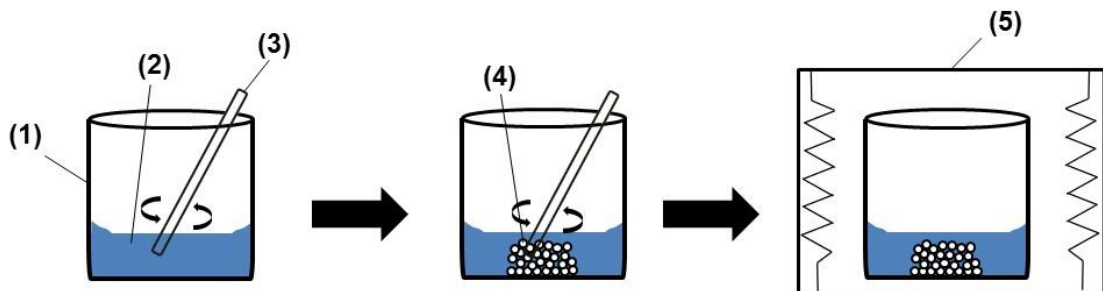
Figure. 4.1 Preparation steps for voids embedded hollow capsule: (1) Glass beaker, (2) Solution, (3) Dispensing spoon, (4) Hollow capsules and (5) Furnace

Table. 4.3 Initial mixture weight ratio

Raw material	Metal nitrates	Urea	Water	PVA	Hollow capsule
Ratio [wt. %]	35	12	20	1	32

Table. 4.4 Metal nitrates weight ratios as raw materials for each sample

Sample name / Metal nitrate	Ni-Co-O				Mg-Al-Fe-O	
	—	*Ce*	*Mg*	*Mg-Al*	—	*Co*
$Ni(NO_3)_2\ 6H_2O$	40	33.3	20	20	—	—
$Co(NO_3)_2$	60	50	30	30	—	30
$Ce(NO_3)_3\ 6H_2O$	—	16.7	—	—	—	—
$Mg(NO_3)_2\ 6H_2O$	—	—	50	13.8	13.8	13.8
$Al(NO_3)_3\ 9H_2O$	—	—	—	36.2	36.2	36.2
$Fe(NO_3)_3\ 9H_2O$	—	—	—	—	50	20

(wt. %)

4.2.2 Gas exposure test

The shell structure modified capsule was exposure to the gas flowing and heating condition as follows: Firstly, a small amount of refractory wool was put in a quartz tube with 10 mm widths and 635 mm lengths at around the center of the quartz tube. Then, 2.2 ml of shell structure modified hollow capsules sample were put in the quartz tube and small amount of refractory wool was also put at another edge of sample to prevent the sample from being blown off during the gas flow. Secondly, the quartz tube contained the sample and refractory wools was set in a tubular furnace. One edge of the quartz tube was connected with a hose to flow gases (i.e. Inflow gases). Another edge of the quartz tube was also connected with another hose to flow gases passed through the sample and water with ice cooling trap (i.e. Outflow gases). Inflow gases

including equal volume of methane, carbon dioxide and nitrogen were flowed with 0.2 liter gases per liter of sample per second. Lastly, the tubular furnace was heated up to 1,023 K prior to flowing the gases. The temperature was varied from 1,023 K to 1,173 K during the gas flowing and kept for 10 minutes at specific temperature for a gas analysis described in 4.2.2. After reaching to maximum temperature, the inflow gases were stopped to flow and sample was naturally cooled down to room temperature. A total time for the gas flowing under the heating condition in the range of temperature as mentioned above was less than 3 hours. Experimental setup was given in Figure 4.2 to understand intuitively.
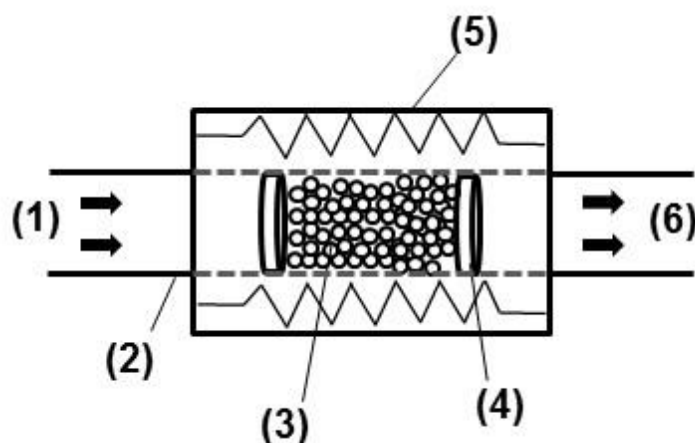
Figure. 4.2 Experimental setup for gas exposure test: (1) Inflow gases, (2) Quartz tube, (3) Sample, (4) Refractory wool, (5) Tubular furnace and (6) Out flow gases

4.2.3 Characterization

Morphologies of shell structure modified hollow capsule were observed by SEM (JSM-6610LA, JEOL) to observe how powder embedded on the shell. All samples were sputtered with Au for a conductivity imparting prior to the SEM analysis. Specific surface areas of samples were calculated from BET method based on a measurement of nitrogen gas adsorption (BELSORP-28SA, MicrotracBEL Corp.) at 77 K. Total pore volumes of samples were also calculated from a maximum nitrogen adsorbed amount. Prior to nitrogen adsorption analysis, all samples were dried at 333 K for 24 hours and

heated at 573 K for 200 min. to remove adsorbed water on the surface. Crystal forms of samples were analyzed by an x-ray diffractometer (XRD, Siemens D500) with a CuKα emission wavelength, 0.03 deg. scan step and 1.7 deg./min. scan speeds. Each sample mixed with 10 wt. % of a potassium chloride (KCl) was used for the XRD analysis. KCl was used for a reference material to obtain the specific diffraction intensity at an intrinsic angle. Elemental analysis for samples was analyzed by an energy dispersive x-ray spectroscopy (EDS) attached to SEM.

0.6 ml of outflow gases were collected during the heating sample and flowing the inflow gases at 10 minutes after reaching to a specific temperature. The collected outflow gases were analyzed by a gas chromatography (GC 86.10, DANI) with a thermal conductivity detector, a polymer HaySep Q 80 / 100 mesh column heated at 363 K and a helium carrier gas flowed in 30 milliliter per minutes. The catalytic performance of each sample was evaluated with gas decreasing rate [%] of methane and carbon dioxide and the ratio between each gas decreasing rate by using equations as follows:

$$CH_4 \text{ decreasing rate} = (CH_{4in} - CH_{4out}) / CH_{4in} \times 100 \tag{7}$$

$$CO_2 \text{ decreasing rate} = (CO_{2in} - CO_{2out}) / CO_{2in} \times 100 \tag{8}$$

$$\text{Ratio of gases decreasing rate} = CH_4 \text{ decreasing rate} / CO_2 \text{ decreasing rate} \tag{9}$$

where CH_{4in} [a.u.] and CO_{2in} [a.u.] are initial amount of methane and carbon dioxide in inflow gases analyzed by the gas chromatography, respectively. CH_{4out} [a.u.] and CO_{2out} [a.u.] are amount of methane and carbon dioxide in outflow gases analyzed by the gas chromatography, respectively. If small amount of gases are obtained in outflow gases and a ratio between the decreasing rates of methane and carbon dioxide is close to 1, it can reveal that these gases are converted to hydrogen and carbon monoxide. This estimation is based on stoichiometric proportion that a chemical reaction formula for this conversion process can be expressed as $CH_4 + CO_2 \rightarrow 2H_2 + 2CO$. Morphologies

and crystal forms of samples after the gas exposure test were also investigated by SEM and XRD with same conditions as mentioned above.

4.3 Results and discussion

4.3.1 Morphology, elemental composition and gas adsorption of voids embedded hollow capsule

All samples of shell surface modified hollow capsules retained its hollow spherical shape although the high temperature reaction during the modification was occurred with multiple gas bi-products dispersion. The products powder with dozens of micrometer size were partly covered the hollow capsule as shown in Figure 4.3-a. As can be seen from EDS spectra analyzed for 2 areas with different appearances (Figure 4.4), the area indicated as EDS 1 had the compositions originated mainly in the original composition of hollow capsule (Sr, Fe and O), the other area indicated as EDS 2 had the compositions originated mainly in the embedded powder (Ni, Co, Mg, Al and O). Furthermore, the embedded powder also partly existed in inner surface of shell according to the images (Figure 4.3-a) and EDS spectra (Figure 4.5). It can be considered that the solution mixture contained raw materials permeated into the core of hollow capsule through the voids between particles and the reaction partially occurred.
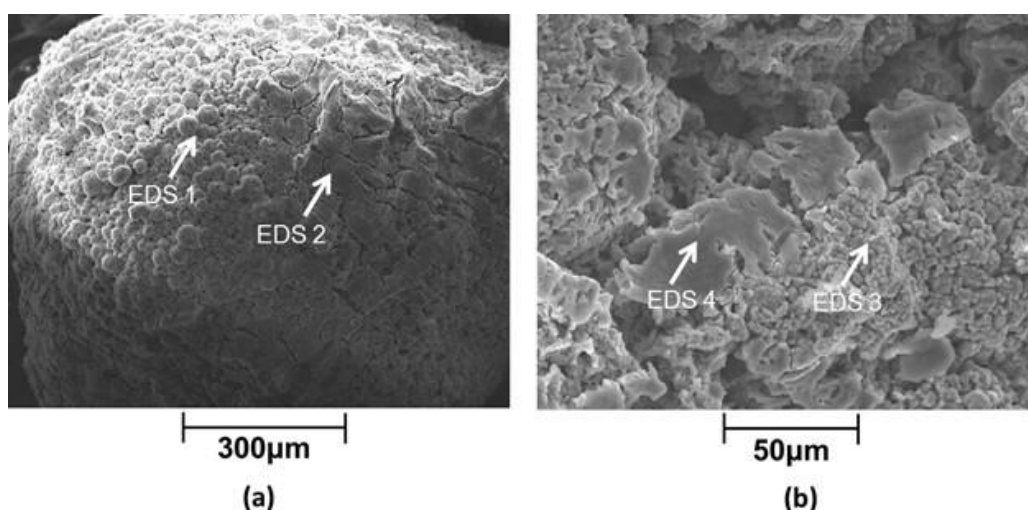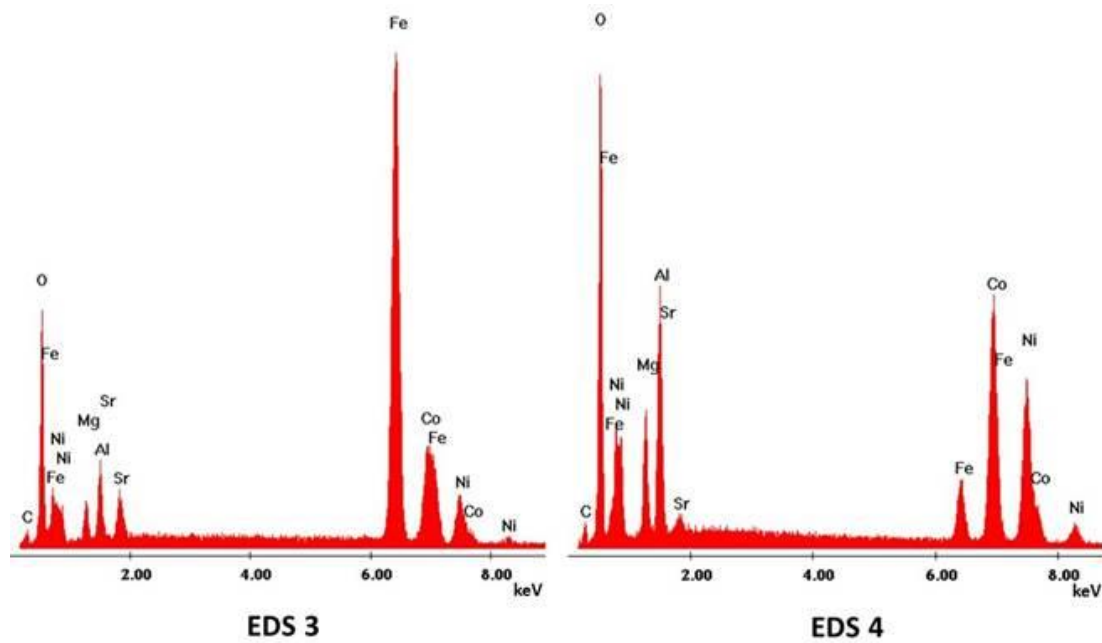

Figure. 4.3 SEM images of outer surface (a) and inner surface (b) of voids embedded hollow capsule (Ni-Co-Mg-Al-O sample)
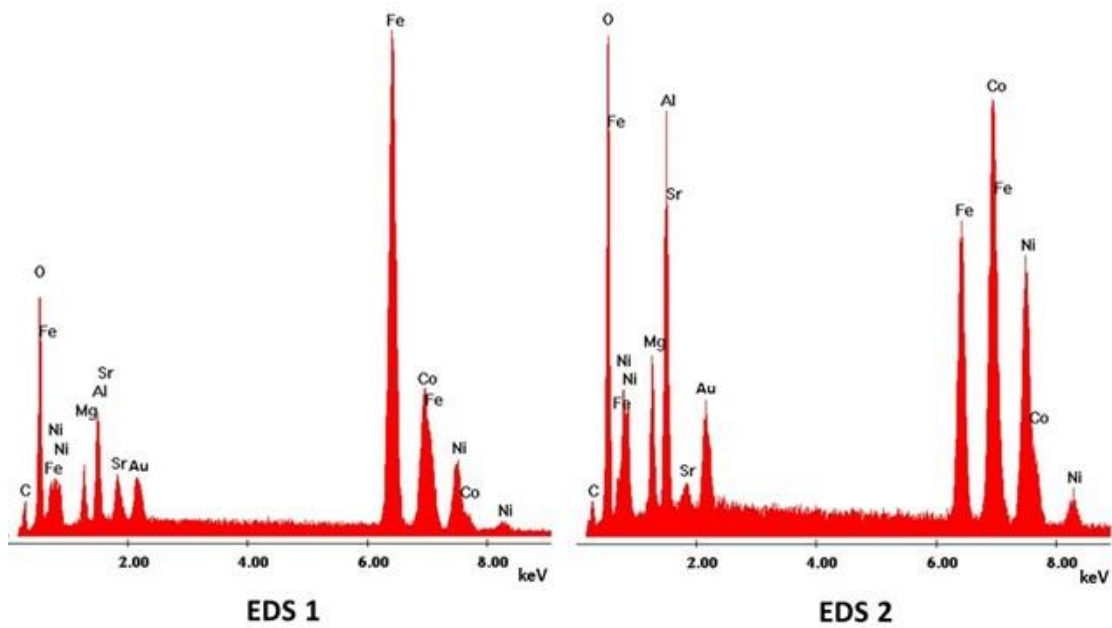
Figure. 4.4 EDS spectra of outer surface of voids embedded hollow capsule (Ni-Co-Mg-Al-O sample) (Numbers are corresponded to indicated area shown in Figure 4.3-a)

Figure. 4.5 EDS spectra of inner surface of voids embedded hollow capsule (Ni-Co-Mg-Al-O sample) (Numbers are corresponded to indicated area shown in Figure 4.3-b)

High magnification image of surface of voids embedded hollow capsule highlights the morphology of embedded powder on strontium ferrite particle as shown in Figure 4.6-b. The appearance was totally different from the image of hollow capsule without embedding (Figure 4.6-a). The powder embedded the voids between strontium ferrite particles and covered the surface of strontium ferrite particles. In particular, some part of voids changed the size from a few micro meters to hundreds nano meters by embedding of powder. A nonhomogeneous embedding morphology was due to the nonhomogeneous placement of strontium ferrite particles. In spite of low homogeneity of the original morphology, embedded powder could be placed between strontium ferrite particles as well as on the particles. The embedding morphology of all other samples was similar to that of Ni-Co-Mg-Al-O sample.
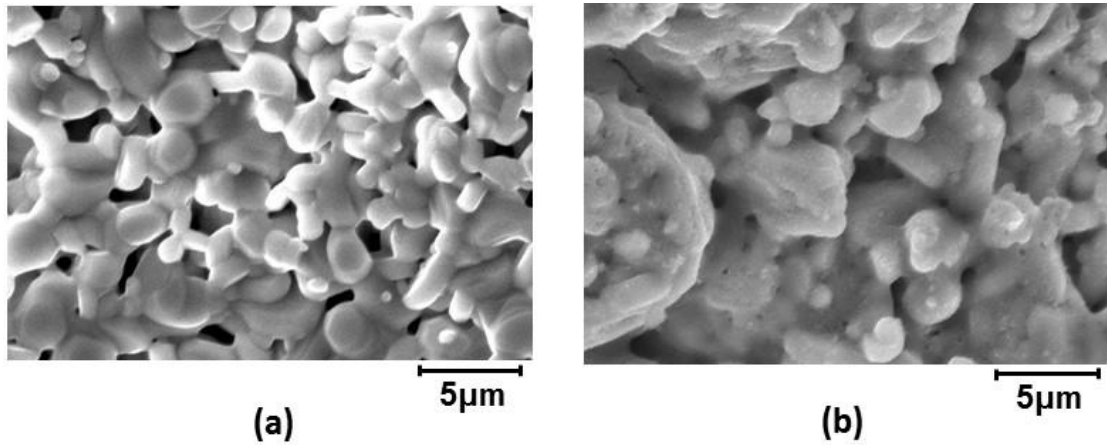

Figure. 4.6 High magnification SEM image of outer surface of hollow capsule without embedding (a) and voids embedded hollow capsule (Ni-Co-Mg-Al-O sample, b)

Figure 4.7 and 4.8 shows that the each elemental composition of embedded powder existed inside the shell as indicated with red square parts on the spectra. Figure 4.7 also shows that the embedded powder covered the shell of hollow capsule with the thickness of a few micro meters. This covered morphology was especially observed in outside shell. It is proved that the embedding powder tended to place on the outside shell due to poor immersion of raw materials solution into the core. Besides, Figure 4.8

also shows low oxygen intensities over the entire shell compared with those before gas exposure test. Further discussion for this result in terms of crystal form change due to gas exposure is described in 4.3.3.
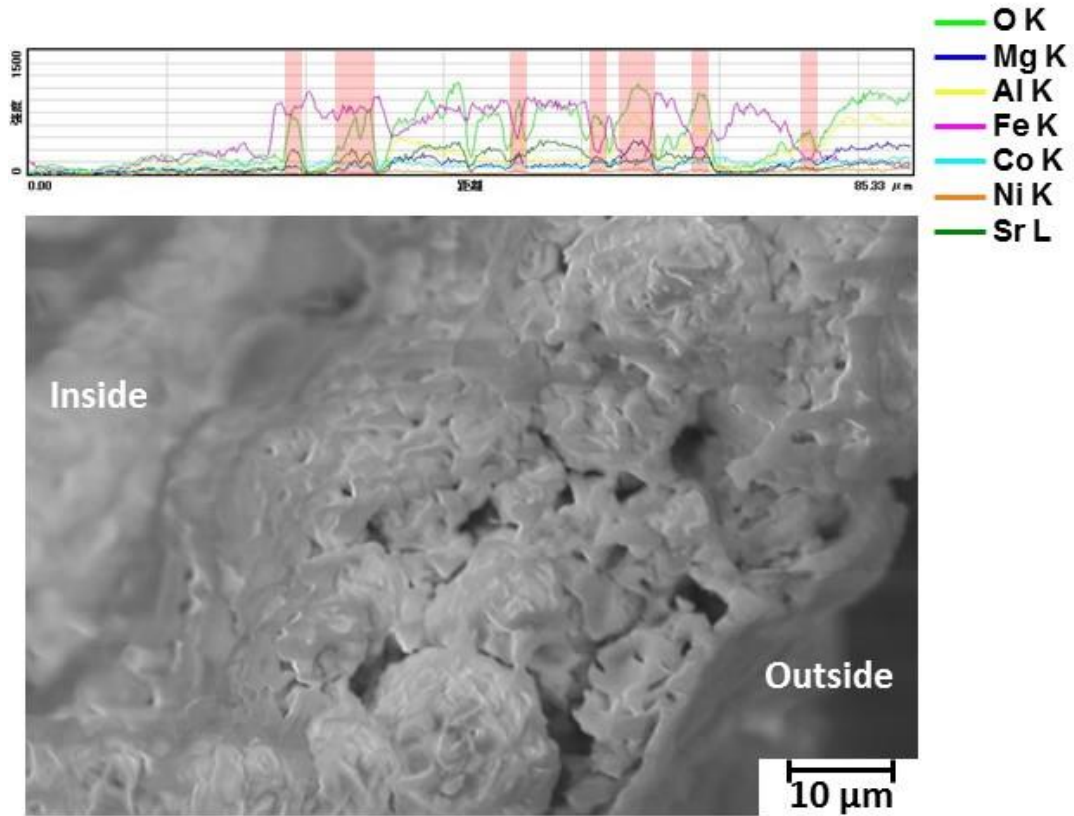
Figure. 4.7 EDS line analysis spectra at cross-sectional area of voids embedded hollow capsule (Ni-Co-Mg-Al-O sample)
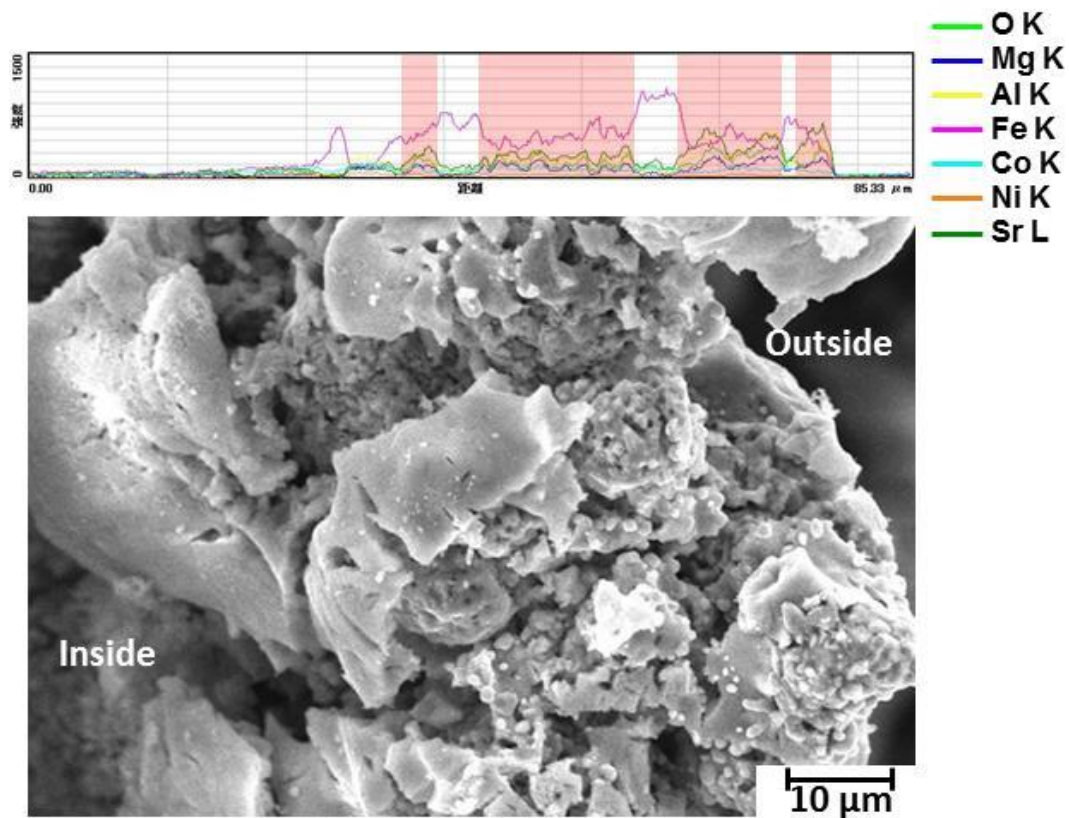
Figure. 4.8 EDS line analysis spectra at cross-sectional area of voids embedded hollow capsule (Ni-Co-Mg-Al-O sample) after gas exposure test

The specific surface area and total pore volume of each sample were mostly less than those of original hollow capsule as described in Table 4.5. The results indicate that the amount of nitrogen gas adsorbed on the surface decreased because of the closing of voids and pores on the hollow capsules by embedding powder. The effect of embedding of powder on the promotion of closing of voids and pores would be dominated rather than the heating process during the SCS process. The difference of specific surface areas among samples was larger than that of total pore volumes. It means that voids between strontium ferrite particles were intensively closed compared with pores on the particles.

Table. 4.5 Specific surface area and total pore volume of voids embedded hollow capsules for each sample and hollow capsule sintered at 1,373 K without surface modification.

| Sample No.	Specific surface area [m^2/g]	Total pore volume [cm^3/g]
1	5.6	0.016
2	10.8	0.017
3	7.5	0.018
4	19.4	0.018
5	10.7	0.013
6	13.3	0.020
Hollow capsule	22.8	0.020

4.3.2 Gas decreasing rates

Methane and carbon dioxide decreasing rates highly depended on the samples as shown in Figure 4.9 and 4.10. Besides, Figure 4.11 shows that the ratio of methane decreasing rate and carbon dioxide decreasing rate for all samples. Ni-Co-O based samples with additives exhibited high decreasing rates more than 80 % and showed the ratio of approximately 1. It can be said that those samples had high activities to convert the gases to hydrogen and carbon monoxide. The carbon dioxide decreasing rates of them and methane decreasing rate of Ni-Co-Ce-O sample moderately increased as increasing the temperature. On the other hand, Ni-Co-O sample, Mg-Al-Fe-O sample and Mg-Al-Fe-Co-O sample exhibited low decreasing rates compared with those of Ni-Co-O based samples with additives. The ratio of gases decreasing rate for these

samples increased with increasing the temperature. At lower temperature, the ratios for them were below 1 which means that other reactions such as methanation ($CO + 3H_2 \rightarrow$ $CH_4 + H_2O$, $CO_2 + 4H_2 \rightarrow CH_4 + 2H_2O$) or reverse gas shift reaction ($CO_2 + H_2 \rightarrow CO$ $+ H_2O$) would additionally occurred. At higher temperature, the ratios for Ni-Co-O sample and Mg-Al-Fe-O sample were above 1 which also means other reactions such as steam reforming reaction ($CH_4 + H_2O \rightarrow 3H_2 + CO$), methane combustion ($CH_4 +$ $2O_2 \rightarrow CO_2 + 2H_2O$) or gas shift reaction ($CO + H_2O \rightarrow CO_2 + H_2$) would additionally occurred. Although Ni-Co-O sample had similar crystal forms to Ni-Co-O based samples with additives except cerium, magnesium and aluminium, it exhibited the decreasing rates less than 40 %. It can be said that those additional compositions would promote the conversion performance. The methane decreasing rates of Ni-Co-O sample and Mg-Al-Fe-O sample increased and the carbon dioxide decreasing rates of the samples decreased as the temperature increases. It can be explained that carbon dioxide is too stable to occur the desired reaction compared with methane, or generated by associated reactions mentioned above such as methane combustion and water gas shift.
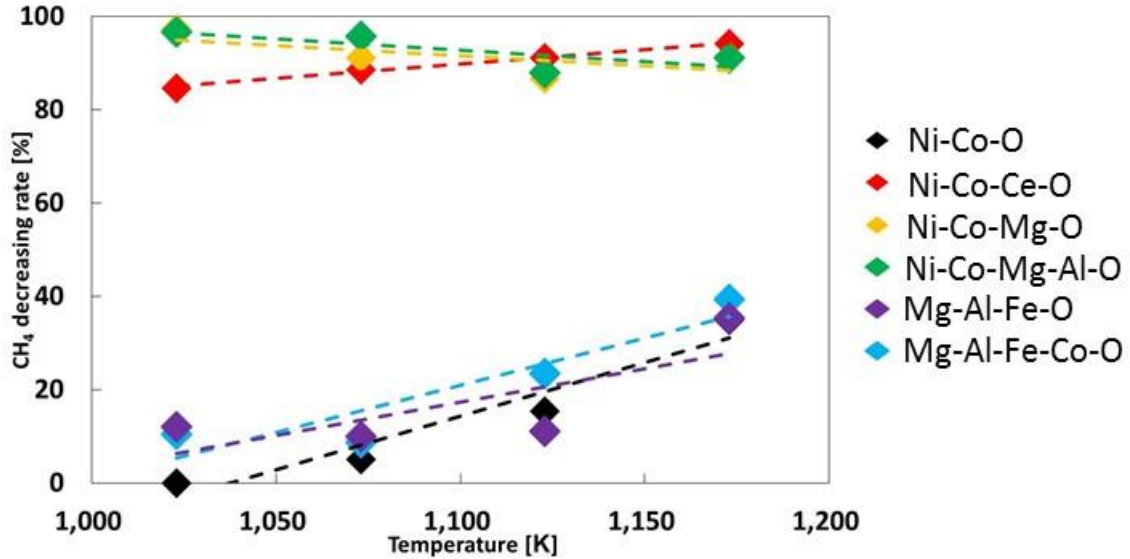
Figure. 4.9 Methane decreasing rates of voids embedded hollow capsules for each sample
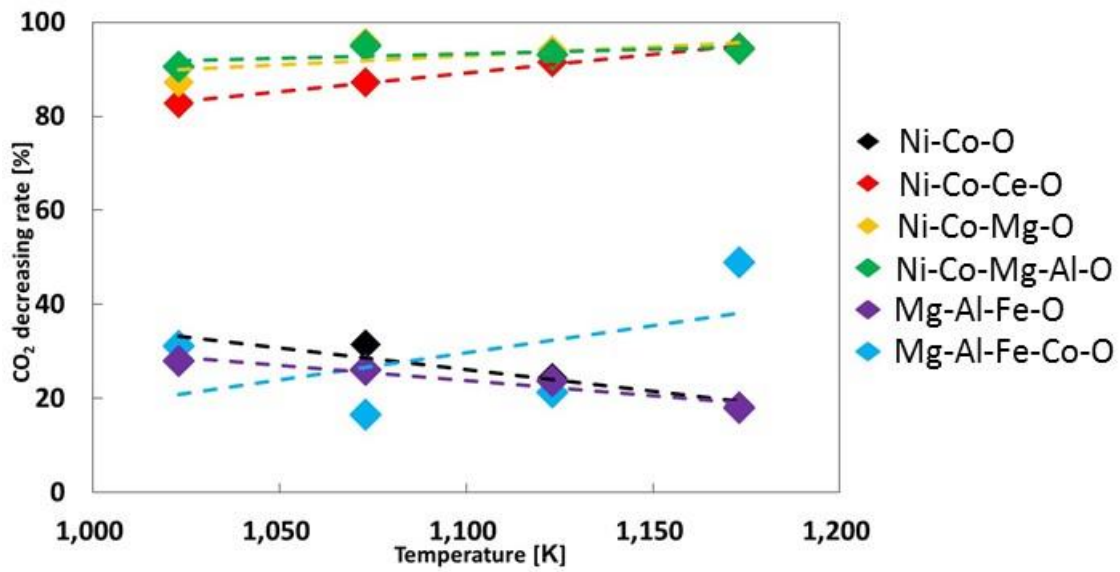
Figure. 4.10 Carbon dioxide decreasing rates of voids embedded hollow capsules for each sample
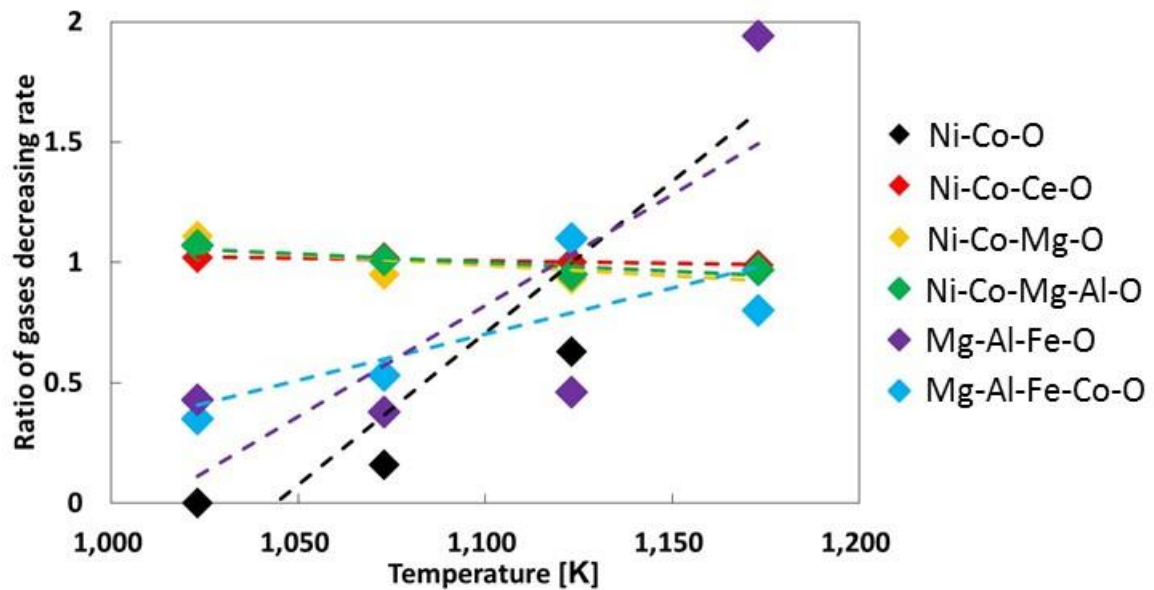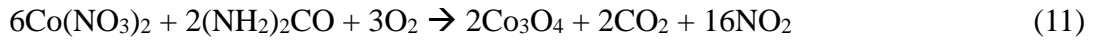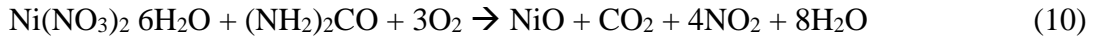

Figure. 4.11 Ratio of decreasing rate of methane and carbon dioxide of voids embedded hollow capsules for each sample

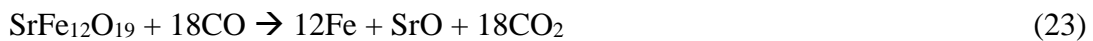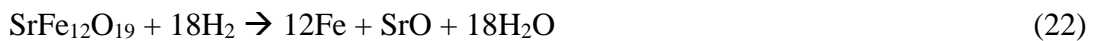4.3.3 Crystal form of voids embedded hollow capsule before and after gas exposure test

Figure 4.12 to Figure 4.17 show XRD spectra and lists of crystal forms which can be considered to exist for all samples of original after gas exposure test. The word

of "original" indicates the crystal structure composition of voids embedded hollow capsule which was not processed the gas exposure test. In this section, reaction processes during SCS and gas exposure test for each sample which can be considered to occur were discussed.

The crystal forms of Ni-Co-O sample appeared through following processes except strontium ferrite:

$$Ni(NO_3)_2\ 6H_2O + (NH_2)_2CO + 3O_2 \rightarrow NiO + CO_2 + 4NO_2 + 8H_2O \qquad (10)$$

$$6Co(NO_3)_2 + 2(NH_2)_2CO + 3O_2 \rightarrow 2Co_3O_4 + 2CO_2 + 16NO_2 \qquad (11)$$

$$NiO + Co_3O_4 \rightarrow Co_2NiO_4 + CoO \qquad (12)$$

These materials synthesized by SCS process while crystal structure of hollow capsule retained. It means that strontium ferrite was stable in this process. Some spectra in Figure 4.12 were overlapped by multiple crystal phases. On the other hand, the crystal forms of Ni-Co-O sample after gas exposure test were different from those of original compositions. Following processes are considered reactions during the gas exposure test which caused the variation of crystal forms:

$$CH_4 + CO_2 \rightarrow 2H_2 + 2CO \qquad (13)$$

$$NiO + H_2 \rightarrow Ni + H_2O \qquad (14)$$

$$NiO + CO \rightarrow Ni + CO_2 \qquad (15)$$

$$Co_3O_4 + 4H_2 \rightarrow 3Co + 4\ H_2O \qquad (16)$$

$$Co_3O_4 + 4CO \rightarrow 3Co + 4CO_2 \qquad (17)$$

$$CoO + H_2 \rightarrow Co + H_2O \qquad (18)$$

$$CoO + CO \rightarrow Co + CO_2 \qquad (19)$$

$$Co_2NiO_4 + 4H_2 \rightarrow 2Co + Ni + 4H_2O \qquad (20)$$

$$Co_2NiO_4 + CO \rightarrow 2Co + Ni + 4CO_2 \qquad (21)$$

$$SrFe_{12}O_{19} + 18H_2 \rightarrow 12Fe + SrO + 18H_2O \qquad (22)$$

$$SrFe_{12}O_{19} + 18CO \rightarrow 12Fe + SrO + 18CO_2 \qquad (23)$$

It is considered that the various metals appeared by a hydrogen or carbon monoxide reduction. The hydrogen and carbon monoxide are considered as a reducing agent in

this system. Ni-Co-O sample exhibited low catalytic activity compared with other samples, however, the hydrogen and carbon dioxide were converted from the methane and carbon dioxide. Besides, its activity retained although the crystal form was changed. It can be said those metals was key materials as the catalysts. According to these processes, a lot of water and carbon dioxide were produced as the bi-products. However, no water was collected in the cooling trap during the gas exposure test. It can be due to that small amount of sample were used. The produced carbon dioxide would be detected with the carbon dioxide in inflow gases. In fact, the decreasing rate of carbon dioxide of Ni-Co-O sample decreased as the temperature increases, on the other hand that of the methane increased with increasing the temperature (Figure 4.9 and 4.10). Unfortunately, the process step as a function of time could not precisely discussed with the results, however, the reduction processes during the gas exposure condition were intensively occurred by carbon monoxide. Interestingly, the strontium ferrite was also changed to iron and strontium oxide. The spectra of strontium oxide were not observed due to small weight ratio in the strontium ferrite. As a result of preliminary experiment, the crystal structure of hollow capsule without any shell modification which was exposure to gas flowing under same condition described in 4.2.2 was also reduced to strontium oxide and iron oxides. It can be proved the existence of strontium oxide, simultaneously, the hollow capsule itself can convert the gases. Although crystal form of sample intensively changed, the hollow spherical shape of sample retained.
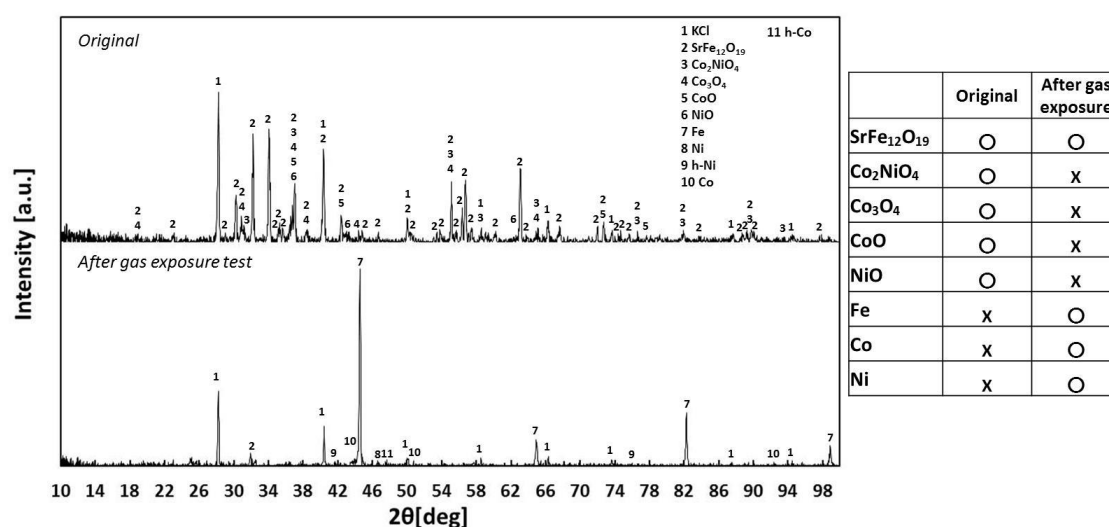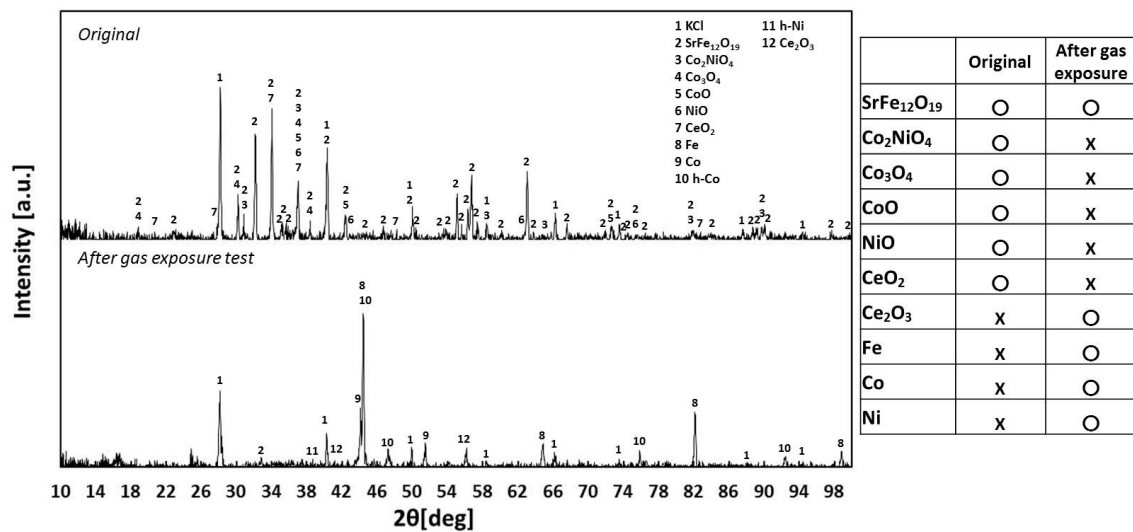
Figure. 4.12 XRD spectra and crystal forms of voids embedded hollow capsules for Ni-Co-O

sample of original and after gas exposure test ("O" indicates that the diffraction intensity of crystal

form was observed, "X" indicates that the any diffraction intensities of crystal form were not

observed.)

Some of crystal forms of Ni-Co-Ce-O sample were similar to those of

Ni-Co-O sample except cerium oxide as shown in Figure 4.13. It was appeared through

following process:

$$Ce(NO_3)_2\ 6H_2O + (NH_2)_2CO + O_2 \rightarrow CeO_2 + CO_2 + 5NO_2 + 8H_2O \qquad (24)$$

Other compositions were produced via same processes as described for Ni-Co-O sample.

After the gas exposure test, most of crystal forms were reduced to metals by similar

process conditions as described for Ni-Co-O sample. However, both of hydrogen and

carbon monoxide can be considered to play a role as the reduction center. Because the

methane and carbon dioxide decreasing rates for Ni-Co-Ce-O sample were equivalently

high. Higher decreasing rates were achieved by the existence of cerium oxide. The

cerium oxide can promote the active site of metals by oxygen storage and transport

function [9]. In the oxidation and reduction environments, cerium inside its oxide

promotes an electric transfer and produces the redox power. As a result, the crystal form

after gas exposure test included cerium (III) oxide instead of cerium (IV) oxide.

Original

1 KCl 11 h-Ni
2 $SrFe_{12}O_{19}$ 12 Ce_2O_3
3 Co_2NiO_4
4 Co_3O_4
5 CoO
6 NiO
7 CeO_2
8 Fe
9 Co
10 h-Co

After gas exposure test

Intensity [a.u.]

2θ[deg]

	Original	After gas exposure
$SrFe_{12}O_{19}$	O	O
Co_2NiO_4	O	x
Co_3O_4	O	x
CoO	O	x
NiO	O	x
CeO_2	O	x
Ce_2O_3	x	O
Fe	x	O
Co	x	O
Ni	x	O

Figure. 4.13 XRD spectra and crystal forms of voids embedded hollow capsules for Ni-Co-Ce-O sample of original and after gas exposure test
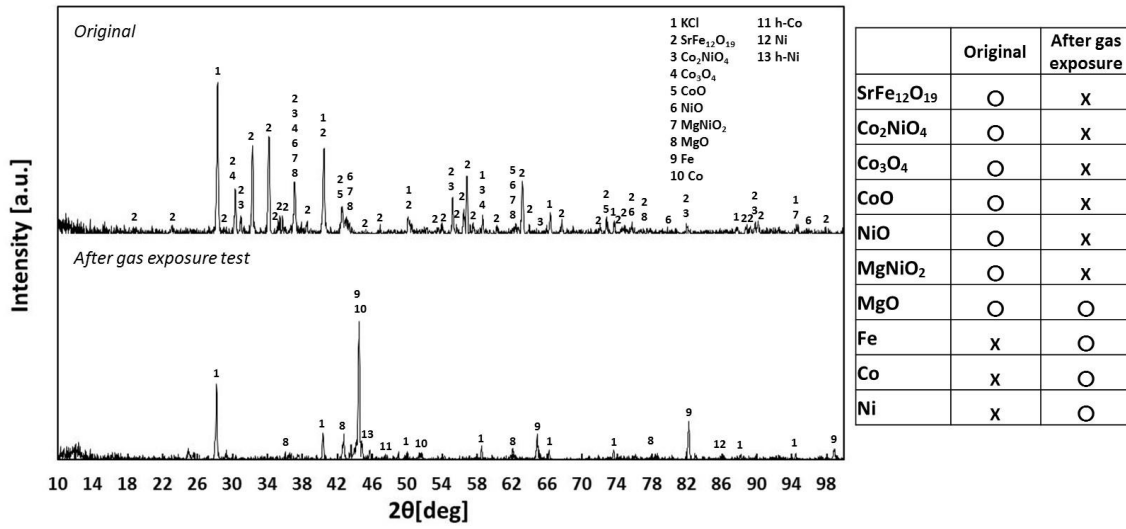
As for the Ni-Co-Mg-O sample (Figure 4.14), the crystal forms based on the magnesium were produced with other similar compositions described above. They were appeared through following processes:

$$Mg(NO_3)_2\ 6H_2O + (NH_2)_2CO + 3O_2 \rightarrow MgO + CO_2 + 4NO_2 + 8H_2O \qquad (25)$$

$$NiO + MgO \rightarrow MgNiO_2 \qquad (26)$$

Most of results and discussion were same as those for Ni-Co-Ce-O sample except that related to cerium oxide. The structure consisted of nickel and magnesium is produced. Subsequently, this structure changed to magnesium oxide and nickel via reduction processes by the hydrogen and carbon monoxide.
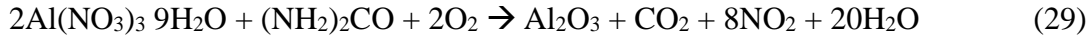
$$MgNiO_2 + H_2 \rightarrow MgO + Ni + H_2O \qquad (27)$$

$$MgNiO_2 + CO \rightarrow MgO + Ni + CO_2 \qquad (28)$$

However, the magnesium oxide retained its composition even after the gas exposure test as shown in Figure 4.14 It can be considered that the magnesium oxide has high material stability under the experimental condition. Besides, the magnesium oxide would play significant role as a support material to promote the active site of metals.
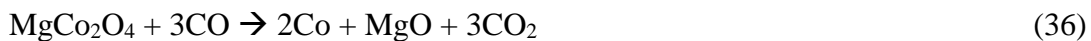
Figure. 4.14 XRD spectra and crystal forms of voids embedded hollow capsules for Ni-Co-Mg-O sample of original and after gas exposure test

The crystal forms based on the aluminium were produced with other similar compositions described above for Ni-Co-Mg-Al-O sample (Figure 4.15). They were appeared through following processes:

$$2Al(NO_3)_3 \ 9H_2O + (NH_2)_2CO + 2O_2 \rightarrow Al_2O_3 + CO_2 + 8NO_2 + 20H_2O \qquad (29)$$

$$CoO + Al_2O_3 \rightarrow CoAl_2O_4 \qquad (30)$$

$$MgO + Al_2O_3 \rightarrow MgAl_2O_4 \qquad (31)$$

$$Co_3O_4 + MgO \rightarrow MgCo_2O_4 + CoO \qquad (32)$$

It is considered that the Ni-Co-Mg-Al-O sample had a lot of spinel structures compared with those of other samples. However, only the magnesium aluminate ($MgAl_2O_4$) could retain its composition after the gas exposure test. This spinel is well-known as a refractory material. It can be said that material stability is high even under the reduction environment. The alumina (α-Al_2O_3) was produced by reduction of other spinel structures and also retained its composition.

$$CoAl_2O_4 + H_2 \rightarrow Co + Al_2O_3 + H_2O \qquad (33)$$

$$CoAl_2O_4 + CO \rightarrow Co + Al_2O_3 + CO_2 \qquad (34)$$

$$MgCo_2O_4 + 3H_2 \rightarrow 2Co + MgO + 3H_2O \qquad (35)$$

$$MgCo_2O_4 + 3CO \rightarrow 2Co + MgO + 3CO_2 \qquad (36)$$
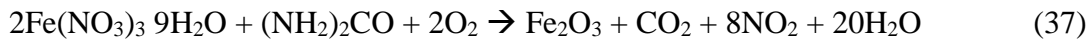
The discussion about high catalytic activity was similar to that of Ni-Co-Mg-O sample.

Those high stability materials kept the good activity of metals during the gas exposure.
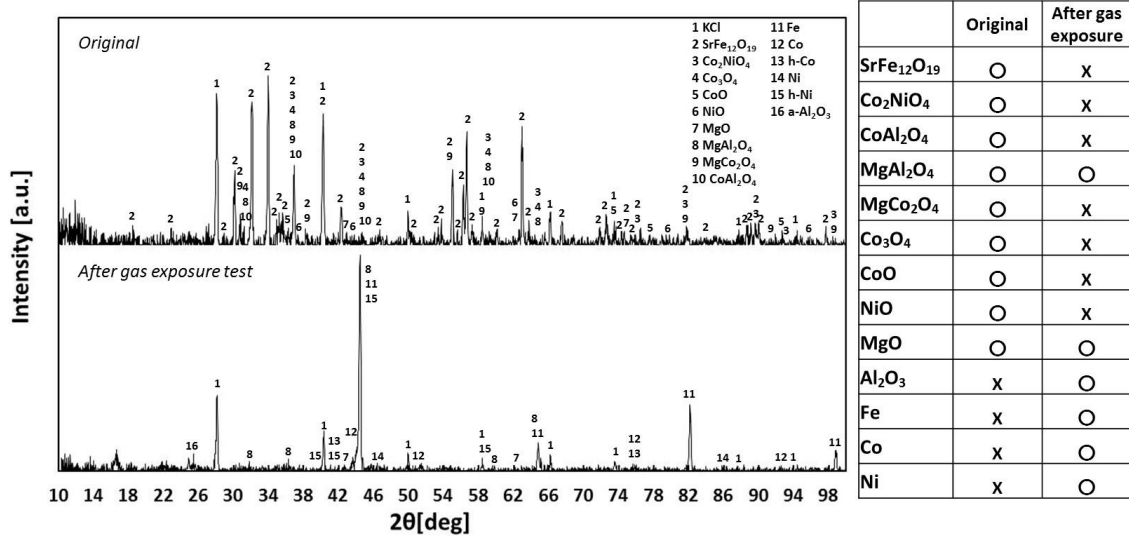
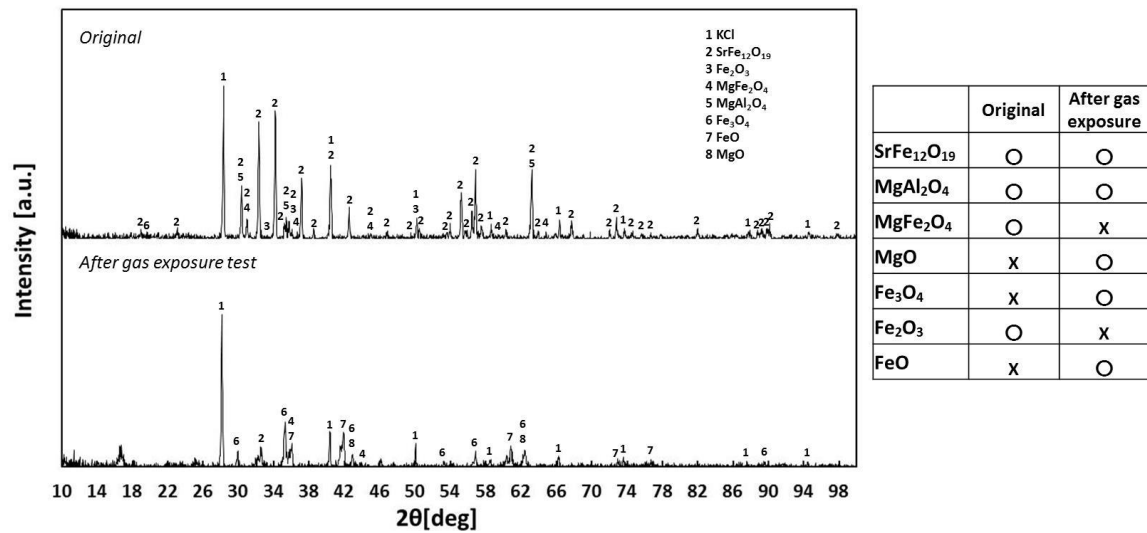**Figure. 4.15** XRD spectra and crystal forms of voids embedded hollow capsules for
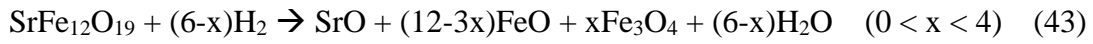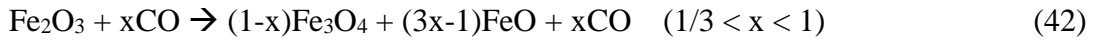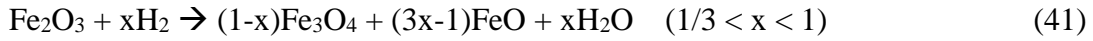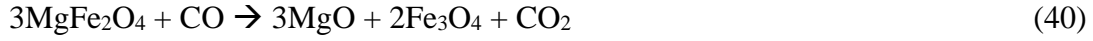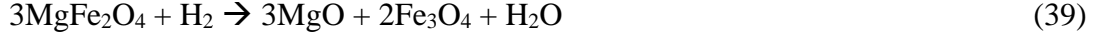
Ni-Co-Mg-Al-O sample of original and after gas exposure test

The crystal forms of Mg-Al-Fe-O sample included the iron based oxides with

other similar compositions described above as shown in Figure 4.16. The production

processes are given here:

$$2Fe(NO_3)_3 \, 9H_2O + (NH_2)_2CO + 2O_2 \rightarrow Fe_2O_3 + CO_2 + 8NO_2 + 20H_2O \quad (37)$$

$$MgO + Fe_2O_3 \rightarrow MgFe_2O_4 \quad (38)$$

The spinel structure consisted of magnesium oxide and iron oxide can be considered to

exist. Subsequently, those compositions with other oxides were reduced to different

crystal form oxides during the gas exposure test. The crystal phase of the strontium

ferrite seemed to remain as detected for the sample after gas exposure test. It can be

explained that small amount of hydrogen and carbon monoxide were produced due to

lower catalytic activity compared. As a result, the reduction processes were moderate.

Although the Mg-Al-Fe-O sample exhibited similar low activity to that of Ni-Co-O

sample, no metals were detected after the gas exposure test. The moderate reduction

process can be considered to be caused by the existence of the iron based oxides in the

76

sample. Because, iron is more stable at reducing environment due to its high ionization energy compared with those of nickel and cobalt: Fe (7.87 eV) > Co (7.86 eV) > Ni (7.64 eV) [10]. The crystal form changes of Mg-Al-Fe-O sample are described as follows:

$$3MgFe_2O_4 + H_2 \rightarrow 3MgO + 2Fe_3O_4 + H_2O \qquad (39)$$

$$3MgFe_2O_4 + CO \rightarrow 3MgO + 2Fe_3O_4 + CO_2 \qquad (40)$$

$$Fe_2O_3 + xH_2 \rightarrow (1-x)Fe_3O_4 + (3x-1)FeO + xH_2O \quad (1/3 < x < 1) \qquad (41)$$

$$Fe_2O_3 + xCO \rightarrow (1-x)Fe_3O_4 + (3x-1)FeO + xCO \quad (1/3 < x < 1) \qquad (42)$$

$$SrFe_{12}O_{19} + (6-x)H_2 \rightarrow SrO + (12-3x)FeO + xFe_3O_4 + (6-x)H_2O \quad (0 < x < 4) \qquad (43)$$

$$SrFe_{12}O_{19} + (6-x)CO \rightarrow SrO + (12-3x)FeO + xFe_3O_4 + (6-x)CO_2 \quad (0 < x < 4) \qquad (44)$$
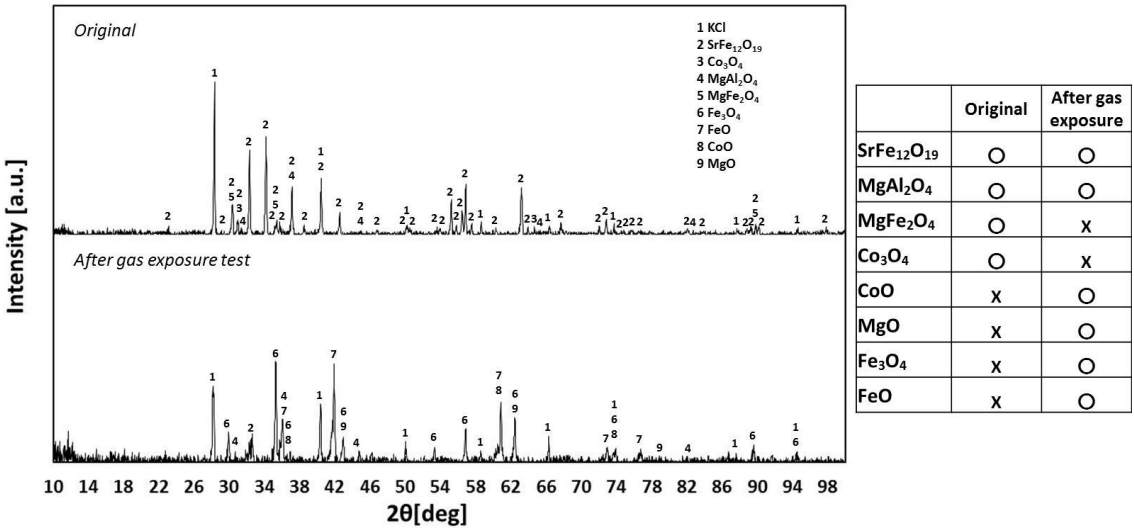

Figure. 4.16 XRD spectra and crystal forms of voids embedded hollow capsules for Mg-Al-Fe-O sample of original and after gas exposure test

The variation of crystal forms of Mg-Al-Fe-Co-O sample (Figure 4.17) was similar to that of Mg-Al-Fe-O sample except containing cobalt based oxide. The cobalt oxide was also reduced to other crystal form of cobalt oxide as follows:

$$Co_3O_4 + H_2 \rightarrow 3CoO + H_2O \qquad (45)$$

$$Co_3O_4 + CO \rightarrow 3CoO + CO_2 \qquad (46)$$

Although cobalt is effective to play role as the active site, the catalytic performance is quite low and similar to that of Mg-Al-Fe-O sample. It can be considered that the amount of cobalt was small which is not enough to promote the catalytic performance.

	Original	After gas exposure
$SrFe_{12}O_{19}$	O	O
$MgAl_2O_4$	O	O
$MgFe_2O_4$	O	x
Co_3O_4	O	x
CoO	x	O
MgO	x	O
Fe_3O_4	x	O
FeO	x	O

Figure. 4.17 XRD spectra and crystal forms of voids embedded hollow capsules for Mg-Al-Fe-Co-O sample of original and after gas exposure test

To sum up the result about high catalytic activity sample such as Ni-Co-O based samples with additives, the gas conversion and reduction process can be visually presented in Figure 4.18. The high catalytic activity was achieved with the combination of metals as main active site and high stability oxides as activity promoter. One of mechanism related to such combination work in the catalysis field is called a spill over [11]. Other samples which showed low catalytic performance can be considered the cause of the lack of active site or activity promoter.
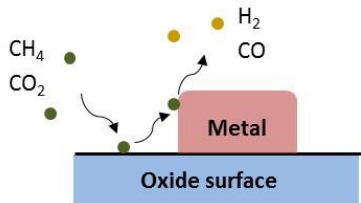
Figure. 4.18 Possible reaction processes for high catalytic performance samples during the gas exposure test

4.4 Conclusions

Voids embedded hollow capsules with multiple oxides including the spinel were successfully produced by SCS technique. The embedded powders were placed at the voids between the particles consisting of hollow capsule shell and broadly existed inside the shell. As a result, the specific surface area and total pore volume for each sample were smaller than those of hollow capsule without the embedding. The methane and carbon dioxide decreasing rates depended on the composition of embedded powders. High decreasing rates more than 80 % were realized with the combination of nickel and cobalt oxides with high stability oxides involving cerium, magnesium and aluminium. The sample containing nickel and cobalt oxide without such high stability oxides had low decreasing rates less than 40 %, although similar intensive composition reduction with those of high decreasing rates samples was observed. The iron based oxide samples had also low decreasing rates with moderate crystal composition reduction due to the high ionization energy of iron. Most of decreasing rates for each sample increased with increasing the temperature during the gas exposure test. The carbon dioxide decreasing rates for some samples decreased with increasing the temperature since other additional reactions would be simultaneously occurred.

References

[1] J. J. Kingsley and K.C. Patil, A novel combustion process for the synthesis of fine particle α-alumina and related oxide materials, *Mater. Lett.*, 6 (11-12) (1988) 427-432

[2] P. Dinka and A. S. Mukasyan, In situ preparation of oxide-based supported catalysts by solution combustion synthesis, *J. Phys. Chem. B*, 109 (2005) 21627-21633

[3] D. Pakhare and J. Spivey, A review of dry (CO_2) reforming of methane over noble metal catalysts, *Chem. Soc. Rev.*, 43 (2014) 7813-7837

[4] G. Xanthopoulou, S. Varitis, K. Karanasios and G. Vekinis, SHS-produced Ni–Co–Al–Mg–O catalysts for dry reforming of methane, *Int. J. Self-Propag. High-Temp Synth.*, 23 (2) (2014) 92-100

[5] N. Sahli, C. Petit, A.C. Roger, A. Kiennemann, S. Libs and M. M. Bettahar, Ni catalysts from $NiAl_2O_4$ spinel for CO_2 reforming of methane, *Catal. Today.*, 113 (2006) 187-193

[6] D. R. Lide, Handbook of chemistry and physics, 72nd edition, special student edition, Boca Raton, Florida USA, CRC press (1991-1992)

[7] D. L. Perry, Handbook of inorganic compounds, 2nd edition, Boca Raton, Florida USA, CRC press (2011)

[8] B. Małecka, A. Łącz, E. Drożdż and A. Małecki, Thermal decomposition of *d*-metal nitrates supported on alumina, *J. Therm. Anal. Calorim.*, 119 (2015) 1053–1061

[9] F. A. J. Al-Doghachi, U. Rashid, Z. Zainal, M. I. Saiman and Y. H. T. Yap, Influence of Ce_2O_3 and CeO_2 promoters on Pd/MgO catalysts in the dry-reforming of methane, *RSC Adv.*, 5 (2015) 81739-81752

[10] J. A. Dean, Lange's handbook of chemistry fifteenth edition, McGRAW-HILL, INC. (1999)

[11] W. C. Conner and J. L. Falconer, Spillover in heterogeneous catalysis, *Chem. Rev.*, 95 (1995) 759-708

Chapter 5 General conclusions

The objectives in the dissertation could be realized and discussed in each chapter as follows.

In chapter 2, the encapsulation of liquid was achieved by using the dry water method where the hydrophobic silica powders coats on the liquid droplet under vigorous blending condition within the short time. The heat transfer through the encapsulated liquids was dominated by thermal conduction while the heat convection in liquid was suppressed due to the isolation of liquid into small area around a few hundred micrometers. The result was confirmed by the comparison of encapsulated thermochromic solution and original solution under heating from bottom of each sample. The encapsulated thermochromic solution changed its color from the bottom as a function of time, on the other hand, the color of original solution without encapsulation changed entirely. Besides, the rate constant in encapsulated solution became larger when larger ratio of hydrophobic silica powders was contained. Smaller capsule size and smaller solution ratio caused decreasing the energy which needs to increase the temperature within the capsule. The thermal transfer in liquid could be controlled by encapsulation of liquid and the results showed the effectiveness to supply the energy to liquid by heating.

In chapter 3, the hollow capsules were successfully produced by the sacrificial template method where the expanded polystyrene beads covered by strontium ferrite powders with polyvinyl alcohol as binder are heated under the melting point of powder. By increasing the sintering temperature within a range from 1,373 K to 1,523 K, capsule size, shell thickness voids area ratio on the shell, specific surface area and total pore volume were simultaneously decreased. The intensive shrinking of capsule and closing of voids or pores on the shell were caused by higher temperature sintering. However, the spherical hollow shape retained independently of the sintering temperature. This elucidation would be effective for the hollow capsule utilization with specific shell porous state.

In chapter 4, the voids in hollow capsule shell sintered at 1,373K were embedded with fine powders produced by solution combustion synthesis. The high temperature within short time during the synthesis could prevent from the void closing due to the sintering of powder particles. The embedded powders partially covered the particles of shell and also placed at between the particles. As a result, the void size in some parts was varied from a few micrometers to hundreds nanometers and specific surface area and total pore volume decreased compared with those of hollow capsule without the embedding. As for the material compatibility under exposure to the methane and carbon dioxide and heating the range from 1,073 K to 1,273 K condition, both of crystal forms of embedded powder and hollow capsule changed by the reduction processes owing to hydrogen and carbon monoxide as the strong reducing agent converted from exposure gases. Although the crystal forms changed, voids embedded hollow capsule involving the nickel, cobalt, cerium, magnesium and aluminium exhibited high gas decreasing rates more than 80 %. The high conversion performance was observed in the combination of nickel and cobalt metals as the active site and cerium, magnesium or aluminium oxides as the promoter for keeping the catalytic activity. Therefore, the catalytic performance was successfully introduced into the hollow capsules. In additions, even though the gas bi-products were observed during the embedding process, and the samples were exposure to methane and carbon dioxide flow under high temperature condition, the hollow spherical shape safely retained. Further experimental conditions such as gas exposure time, gas flow rate or amount of embedded powder should be considered to elucidate, however, the results in this dissertation would be meaningful to give an idea for new utilization of hollow capsule under gas flowing condition as catalyst, catalysts support or adsorbent material. This is the first approach with the hollow capsules produced by the sacrificial template method.

Acknowledgments

I would like to give special thanks to my parents and my relatives for their precious support and advice to the whole of my student life.

Finally, I also would like to thank Japanese Government for an opportunity to apply a tuition exemption system and teaching and research assistant (TRA) system. This research would not have been possible without the financial support.

<div align="right">Ryuma Malik Matsuda</div>

Accomplishments

Publications

1. <u>Ryuma M. Matsuda</u>, Anna V. Gubarevich, Hiroyuki Wada and Osamu Odawara, "Encapsulation of solutions for controlling heat transfer", *Powder Technology*, 268, (2014) 387–391

2. <u>Ryuma M. Matsuda</u>, Galina Xanthopoulou, Hiroyuki Wada and Osamu Odawara, "Characteristic application of ceramic hollow spheres and their qualification", *Advances in Powder Metallurgy & Particulate Materials-2015*, *conference proceedings*, 5, (2015) 72-83

3. <u>Ryuma M. Matsuda</u>, Anna V. Gubarevich, Hiroyuki Wada and Osamu Odawara, "Effect of sintering temperature on the characteristics of ceramic hollow spheres produced by sacrificial template technique", *Ceramics International*, in press, DOI: 10.1016/j.ceramint.2016.02.057

Presentations (international)

1. <u>Ryuma M. Matsuda</u>, Galina Xanthopoulou, Hiroyuki Wada and Osamu Odawara, "Characteristic application of ceramic hollow spheres and their qualification", International Conference on Powder Metallurgy & Particulate Materials POWDERMET2015, San Diego USA, May 17-20, 2015

2. <u>Ryuma M. Matsuda</u>, Galina Xanthopoulou, Hiroyuki Wada, Osamu Odawara and George Vekinis, "Activity of SCS catalysts on hollow spheres in dry reforming of methane", 18th International Symposium on Self-Propagating High Temperature Synthesis - SHS XIII, Antalya Turkey, Oct. 12-15 2015

Contribution

Anna V. Gubarevich, <u>Ryuma. M. Matsuda</u>, Hiroyuki Wada, Galina Xanthopoulou and Osamu Odawara, "A closed circulatory system in space exploration", The Joint Conference of 6th International Symposium on Physical Sciences in Space (ISPS-6) and 10 International conference on Two-Phase Systems for Space and Ground Applications (ITTW2015), Kyoto Japan, Sep. 14-18, 2015

Presentation (domestic)

Ryuma M. Matsuda, Anna V. Gubarevich, Hiroyuki Wada and Osamu Odawara, "Fabrication of high performance ceramic hollow spheres by encapsulating technique", 第52回セラミックス基礎科学討論会, Nagoya Japan, Jan. 9-10, 2014

Fellowship meeting

Ryuma M. Matsuda, "Dry reforming of methane using catalysts on ceramic hollow spheres" Achievements report meeting organized by Innovative Platform for Education and Research (IPER) in Tokyo Institute of Technology, Tokyo Japan, Feb. 20, 2015

Fellowship

1. Grant for students attending international internship from The International Association for the Exchange of Students for Technical Experience (IAESTE), 2012

2. Grant for students attending conference or international workshop from Global COE project (卓越した大学院材料イノベーションのための教育研究拠点), 2014

3. Grant for students attending internship or international workshop from IPER, 2014

Research Internship

1. IAESTE Internship trainee, Department of chemistry, Durham University, Durham England, Aug.-Sep. 2012

2. Visiting researcher, Institute of Nanoscience and Nanotechnology, "Demokritos" National Center for Scientific Research, Athens Greece, Sep.-Dec. 2014